Available online at www.sciencedirect.com

ScienceDirect

Geochimica et Cosmochimica Acta 187 (2016) 350–374

Geochimica et Cosmochimica Acta

www.elsevier.com/locate/gca

# Constraints on formation and evolution of the lunar crust from feldspathic granulitic breccias NWA 3163 and 4881

Claire L. McLeod [a,*], Alan D. Brandon [a], Vera A. Fernandes [b,c,d], Anne H. Peslier [e], Jörg Fritz [f], Thomas Lapen [a], John T. Shafer [a], Alan R. Butcher [g], Anthony J. Irving [h]

[a] *University of Houston, Department of Earth and Atmospheric Sciences, 4800 Calhoun Road, Houston TX 77004, USA*
[b] *Museum für Naturkunde, Leibniz Institute for Research on Evolution and Biodiversity, Invalidenstrasse 43, 10115 Berlin, Germany*
[c] *The Centre for Earth Evolution and Dynamics, University of Oslo, Norway*
[d] *Institute for the Development of New Technologies (UNINOVA), New University of Lisbon, Portugal*
[e] *Jacobs, NASA-Johnson Space Center, Mail Code XI3, Houston, TX 77058, USA*
[f] *Saalbau Weltraum Projekt, Wilhelmstrasse 38, 64646 Heppenheim, Germany*
[g] *FEI Company, Eindhoven, The Netherlands*
[h] *University of Washington, Department of Earth and Space Sciences, Seattle, WA 98195, USA*

Received 25 August 2014; accepted in revised form 19 April 2016; available online 27 April 2016

**Abstract**

Lunar granulitic meteorites provide new constraints on the composition and evolution of the lunar crust as they are potentially derived from outside the Apollo and Luna landing sites. Northwest Africa (NWA) 3163, the focus of this study, and its paired stones NWA 4881 and NWA 4483, are shocked granulitic noritic anorthosites. They are petrographically and compositionally distinct from the Apollo granulites and noritic anorthosites. Northwest Africa 3163 is REE-depleted by an order of magnitude compared to Apollo granulites and is one of the most trace element depleted lunar samples studied to date. New *in-situ* mineral compositional data and Rb–Sr, Ar–Ar isotopic systematics are used to evaluate the petrogenetic history of NWA 3163 (and its paired stones) within the context of early lunar evolution and the bulk composition of the lunar highlands crust. The NWA 3163 protolith was the likely product of reworked lunar crust with a previous history of heavy REE depletion. The bulk feldspathic and pyroxene-rich fragments have $^{87}Sr/^{86}Sr$ that are indistinguishable and average $0.699282 \pm 0.000007$ ($2\sigma$). A calculated source model Sr $T_{RD}$ age of $4.340 \pm 0.057$ Ga is consistent with (1) the recently determined young FAS (Ferroan Anorthosite) age of $4.360 \pm 0.003$ Ga for FAS 60025, (2) $^{142}Nd$ model ages for the closure of the Sm–Nd system for the mantle source reservoirs of the Apollo mare basalts (4.355–4.314 Ga) and (3) a prominent age peak in the Apollo lunar zircon record (*c.* 4.345 Ga). These ages are ~100 Myr younger than predicted timescales for complete LMO crystallization (~10 Myrs after Moon formation, Elkins-Tanton et al., 2011). This supports a later, major event during lunar evolution associated with crustal reworking due to magma ocean cumulate overturn, serial magmatism, or a large impact event leading to localized or global crustal melting and/or exhumation. The Ar–Ar isotopic systematics on aliquots of paired stone NWA 4881 are consistent with an impact event at $\geqslant$ 3.5 Ga. This is inferred to record the event that induced granularization of NWA 3163 (and paired rocks). A later event is also recorded at ~2 Ga by Ar–Ar isotopes is consistent with an increase in the

* Corresponding author at: Department of Geology and Environmental Earth Science, Miami University, 250 S. Patterson Avenue, Oxford, OH 45056, USA.
*E-mail address:* mcleodcl@miamioh.edu (C.L. McLeod).

http://dx.doi.org/10.1016/j.gca.2016.04.032
0016-7037/© 2016 Elsevier Ltd. All rights reserved.

number of impacts on the lunar surface at this time (Fernandes et al., 2013). Northwest Africa 3163 and its paired stones therefore record a *c*. 2.4 Gyr record of lunar crustal production, metamorphism, brecciation, impacts and eventual ejection from the lunar surface.

© 2016 Elsevier Ltd. All rights reserved.

*Keywords:* Lunar crust; Meteorite; Lunar evolution; Geochronology

## 1. INTRODUCTION

Lunar meteorites provide important constraints on the composition of the lunar crust (e.g. Palme et al., 1991; Korotev et al., 2006; Nyquist et al., 2006; Gross et al., 2012; Joy and Arai, 2013; Nagaoka et al., 2013; Boyet et al., 2014; Gross et al., 2014; Borg et al., 2015; Pernet-Fischer and Joy, 2016). These samples are crucial for advancing the understanding of the Moon's geological history. Having been ejected by random impact events on the lunar surface, meteorites potentially offer a broader insight into the petrology, geochemistry and geochronology of the lunar crust than samples obtained by the Apollo and Luna missions.

Northwest Africa (NWA) 3163 and its paired stone NWA 4881 comprise a granulitic noritic anorthosite breccia and are the focus of this study. Together with paired stone NWA 4483, they potentially represent the largest sample of granulitic lunar crust available for study (Irving et al., 2006). Samples are fine-grained, relatively mafic; ~5.8 wt. % FeO, ~5 wt.% MgO and have some of the lowest concentrations of ITE (incompatible trace elements) compared to the feldspathic lunar meteorite suite and returned Apollo and Luna samples (Hudgins et al., 2011a). They are characterized by plagioclase, which has been shocked to maskelynite, pyroxene, olivine, minor chromite and rare Fe–Ti oxide phases. Meteoritic lunar granulites are mineralogically distinct from Apollo granulites in that they lack Fe–Ni grains and contain maskelynite with domains of birefringent plagioclase. For Ca-rich plagioclase ($An_{94}$), this is indicative of shock pressures of 20–24 GPa (Fernandes et al., 2010; Fritz et al., 2011). Granulitic breccias have previously been sampled at several of the Apollo sites in the lunar highlands, typically as small clasts within breccias (77017 and 78155), and as lunar meteorites (Dhofar (Dho) 733 and NWA 5744; Demidova et al., 2007; Hudgins et al., 2008; Kent et al., 2012). Granulitic breccias do not represent primary crystallization products of the Lunar Magma Ocean (LMO) and often have a complex history, including at least one metamorphic event (James et al., 2003; Cohen et al., 2004). In addition, current samples of lunar granulitic breccias likely do not provide a complete record of the lithologic diversity that exists throughout the lunar crust. (Ryder et al., 1997; Korotev et al., 2003).

From previous work, Lunar Ferroan Anorthosite samples (FAS) have been interpreted as potentially representative of early-formed, (LMO)-derived lunar crust (Floss et al., 1998; Norman et al., 2003; Hui et al., 2013). Fig. 1A shows the classic Anorthite-Enstatite (An-En) discrimination diagram for FAS and Mg-suite rocks (high Mg# where

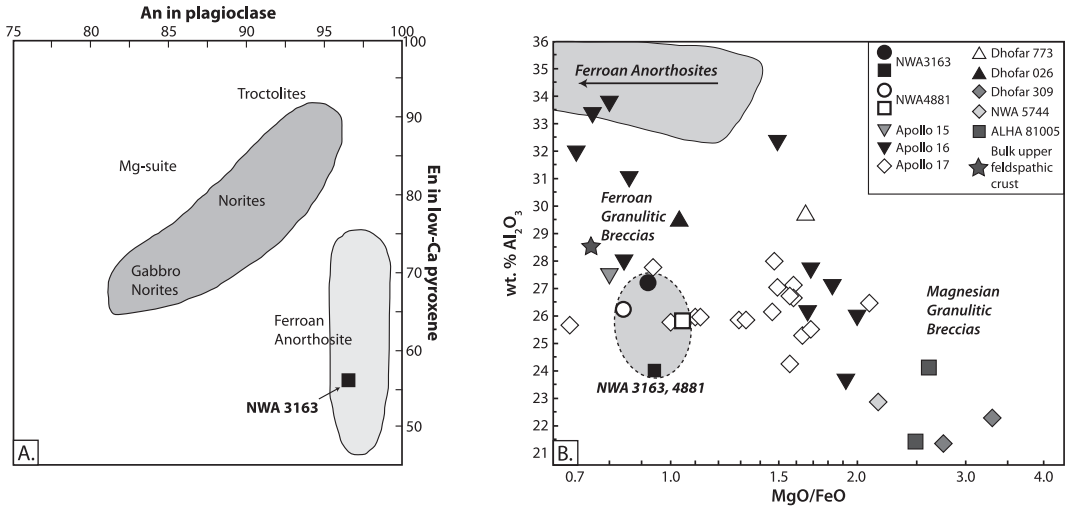


Fig. 1. (A) Classic An-En diagram after James (1980) showing classification of anorthite (An) content in plagioclase and enstatite (En) content of low-Ca pyroxene for lunar highland rock suites. Northwest Africa 3163 shows clear FAS affinity. (B). Classification of NWA 3163 (and paired meteorite 4881) as a ferroan granulitic breccia (noritic anorthosite), using bulk compositions (modified from Hudgins et al. (2011a,b)). Northwest Africa 3163 is shown in the solid circle and square symbols, NWA 4881 in the open circle and square symbols to illustrate the similarities between the paired samples. Lunar meteorites and Apollo Ferroan and Magnesian Breccias are also shown for comparison. Compositional field for Ferroan (MgO/FeO <1.5) and Magnesian (MgO/FeO >1.5) Granulitic Breccias adapted from Hudgins et al. (2011a,b). All breccias are distinct from FAS suite with respect to MgO/FeO vs. wt.% $Al_2O_3$.

Mg# = (Mg/(Mg + Fe)). Northwest Africa 3163 exhibits FAS-affinity with $En_{55}$ in low Ca-pyroxene and high anorthitic plagioclase contents ($An_{94}$). Lunar granulitic breccias are, however, depleted in $Al_2O_3$ with respect to the FAS suite as shown in Fig. 1B. Granulitic breccias are relatively enriched in mafic components with MgO/FeO values ranging from 0.7 to 3.4 and characterized by $Al_2O_3$ contents typically <30 wt.%, with the exception of several Apollo 16 samples (Fig. 1B). In comparison, the FAS suite is characterized by $Al_2O_3$ contents of >30 wt.% and MgO/FeO values <1.5. The MgO/FeO ratios of NWA 3163 and its paired stone 4881 ranges from 0.84 to 1.5 and their bulk-rock wt.% $Al_2O_3$ ranges from 24 to 27.2, classifying it as a ferroan granulitic breccia. It is worth noting, however, that these paired samples exhibit some of the lowest wt.% $Al_2O_3$ contents within the ferroan granulitic breccia suite (Fig. 1B).

Lunar granulites have been sampled as clasts in lunar meteorites (ALH 81005; MAC 88104 and 88105; QUE 93069, Lindstrom et al., 1991; Koeberl et al., 1996; Maloy et al., 2005; Gross et al. 2014), in the Apollo collection (60035, 67415, 67955, 72275, 76503 (Ma and Schmitt, 1982; Lindstrom and Lindstrom, 1986; Salpas et al., 1988; Jolliff et al., 1996; Hudgins et al., 2008) and as rare samples in Apollo regolith fragments (Cushing et al., 1999). This indicates that they are an important component of the lunar crust. The petrogenesis of lunar granulites is broadly associated with impact melting and metamorphism (±partial melting: Warner et al., 1977; Lindstrom and Lindstrom, 1986; Cushing et al., 1999). From textural observations, Cushing et al. (1999) categorized lunar granulitic breccias into three types: poikilitic, poikiltic-granoblastic and granoblastic, each with its own petrogenetic history. Poikilitic breccias were thought to be the result of impact-melting, potentially at larger impact craters (>100 km), where metamorphism has been suggested to have occurred at temperatures of up to 2000 °C, under thick ejecta blankets (2–5 km; Cushing et al., 1999; Hudgins and Spray, 2009) The poikilitic-granoblastic and granoblastic breccias were inferred to have been metamorphosed in the solid-state with burial at shallow levels (cooling at 0.5–50 °C/year at 20–200 m, Cushing et al., 1999). With respect to NWA 3163, Hudgins et al. (2011b) suggested these meteorites formed in 100–200 km craters. Lunar granulitic breccias therefore represent the products of reworked primary lunar igneous lithologies and potentially provide constraints on the composition of the bulk lunar crust.

In order to better understand lunar granulites, this study presents a detailed geochemical and geochronological study of noritic anorthosite NWA 3163, and its paired stone NWA 4881, in order to (1) assess the components in meteoritic lunar granulites and (2) evaluate the petrogenesis of NWA 3163 and its paired stones within the context of lunar evolution. These issues are addressed through *in-situ* measurement of trace elements within constituent minerals and Ar–Ar, Rb–Sr and Sm–Nd isotopic systematics on bulk separates. Throughout this paper, when referring to NWA 3163 and its two paired stones NWA 4881 and NWA 4483, the notation PS is used: NWA 3163 (PS).

## 2. SAMPLE DESCRIPTION

### 2.1. Sample petrography

Northwest Africa 3163 (PS) were found in Mauritania or Algeria in 2005 and have a nearly complete thin, transparent, pale greenish fusion crust (Connolly et al., 2006). The hand samples are composed primarily of plagioclase/maskelynite (~70%), pyroxene (~20%), and olivine (~10%) with accessory Ti-chromite, ilmenite, troilite (FeS) and taenite (Fe, Ni, Irving et al., 2006; Connolly et al., 2008; Fernandes et al., 2009b; Hudgins et al., 2011a,b). These samples are therefore not, *sensu stricto*, anorthosites (>90% plagioclase, Warren, 1990; Boyet et al., 2014).

Multiple shock fractures and thin glass veinlets with rare calcite coatings are also present (see fresh cut of hand specimen; Fig. 2 of Connolly et al., 2006; Irving et al., 2006; Hudgins et al., 2011a,b). Detailed petrographic descriptions of these meteorites are presented in Hudgins et al., 2011a,b. A small slab of NWA 3163, 0.62 cm × 0.61 cm, was selected for a detailed geochemical study and contains lithic and mineral clasts in a fine-grained matrix. Mineral clasts of pyroxene and olivine (<200 μm in diameter) are dispersed throughout the sample. These clasts are more fractured than the mafic phases in the surrounding matrix mafic phases. Fractures in mineral clasts often terminate at grain boundaries, indicating that they may represent an impact event earlier than the one responsible for ejecting the meteorite from the lunar surface. Several of the larger pyroxene grains exhibit fine scale (<5 μm) exsolution lamellae. From intraclast fracture patterns, these phases have previously been interpreted as relict phases which exsolved during slow cooling of the igneous protolith and therefore potentially preserve information regarding the nature of the precursor lithologies to NWA 3163 PS (Hudgins et al., 2011a,b).

A QEMSCAN (Quantitative Evaluation Of Minerals By Scanning Electron Microscopy) image of the studied NWA 3163 chip illustrates the poikiloblastic nature of this sample and was used to quantify its modal mineralogy (Fig. 2). Additional back scattered electron (BSE) images are shown in the Supplementary information. The small slab (0.58 × 0.55 cm) of NWA 3163 of this study contains lithic and mineral clasts in a fine-grained matrix (Supplementary Figs. 1 and 2A–D in SI 1). Matrix mafic phases are typically less than 100 μm in diameter. The matrix is composed predominantly of maskelynite that encloses pyroxene and olivine. Some areas exhibit granoblastic textures (Fig. 2). The largest lithic clast (~1 mm in diameter) is a distinct fine-grained noritic anorthosite clast (mafic phases less than 50 μm in diameter) visible in the lower left part of the slab (Supp. Fig. 2A). Other possible lithic clasts include several maskelynite-rich regions that may be relict anorthosite clasts (Supp. Fig. 2B), a norite clast (Supp. Fig. 2C), and a troctolite clast (Supp. Fig. 2D). The clast shown in Supplementary Fig. 2C is similar to plagioclase-pyroxene intergrowths in Dhofar (Dho) 026 (Cohen et al., 2004), except that the plagioclase in NWA 3163 has been converted to maskelynite, no residual plagioclase laths remain, and these regions typically have irregular margins.

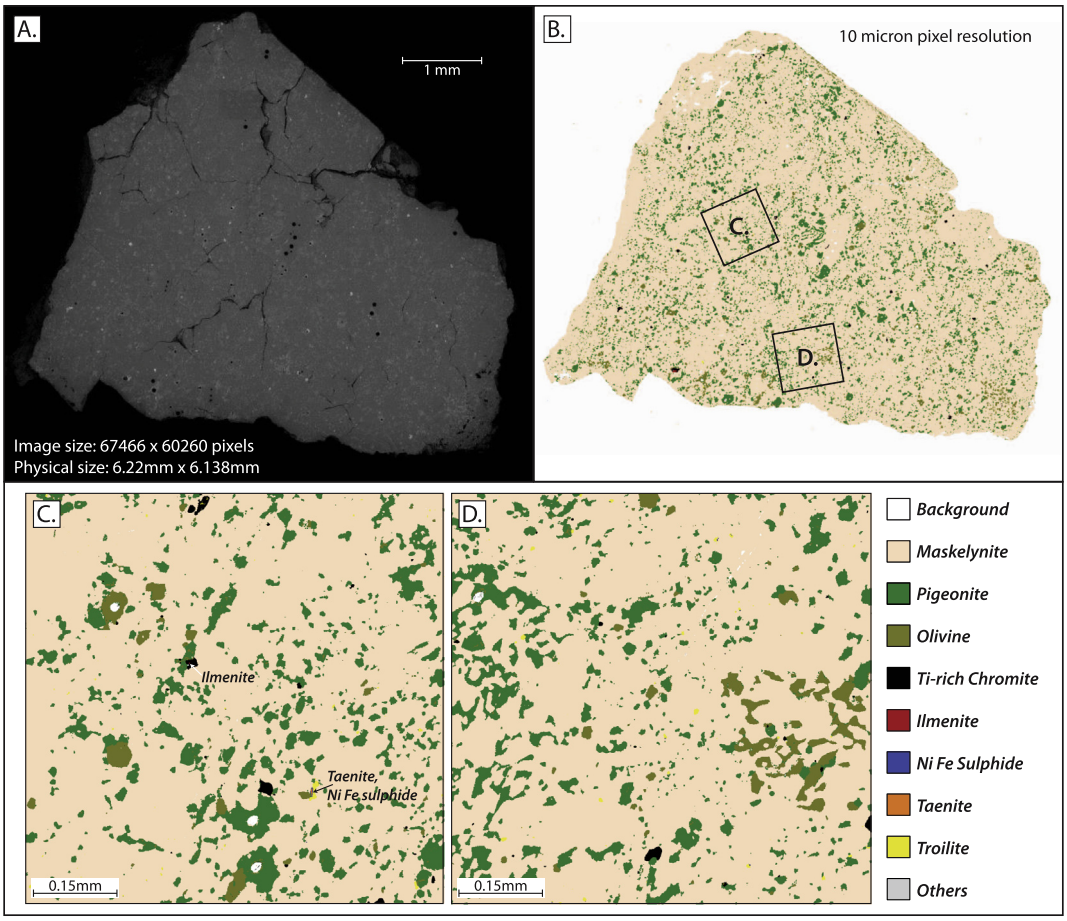


| | Full area (5 microns) | "C" at 1 micron | "D" at 1 micron |
|---|---|---|---|
| **Mineral Volume(%)** | | | |
| *Maskelynite* | 87.4 | 83.9 | 83.1 |
| *Pigeonite* | 9.8 | 13.4 | 12.7 |
| *Olivine* | 2.4 | 2.1 | 3.8 |
| *Ti rich Chromite* | 0.3 | 0.4 | 0.2 |
| *Ilmenite* | <0.01 | <0.01 | nd |
| *Ni Fe Sulphide* | <0.01 | <0.01 | <0.01 |
| *Taenite* | <0.01 | <0.01 | <0.01 |
| *Troilite* | 0.1 | 0.1 | 0.2 |
| *Others* | <0.01 | <0.01 | <0.01 |

Fig. 2. (A) BSE image of studied NWA 3163 chip. (B). QEMSCAN (Quantitative Evaluation of Minerals By Scanning Electron Microscopy) image of studied NWA 3163 chip at 10-micron pixel resolution. Highlighted areas C and D were imaged at 1-micron pixel resolution and are shown in the lower panels.

Many of these clasts do not have sharp boundaries and many grade into the surrounding matrix, making unambiguous identification of lithic clasts difficult. This effect is likely due to recrystallization from thermal metamorphism. Mineral clasts of pyroxene and olivine (less than 200 μm in diameter) are dispersed throughout the sample (Supp. Fig. 3A-D in SI 1). These clasts are significantly more fractured than surrounding matrix mafic phases. It is worth noting that fractures in the mafic mineral clasts often terminate at grain boundaries (Supp. Figs. 3B-D and 4). The QEMSCAN image (Fig. 2) was used to estimate modal proportions, with maskelynite being the most abundant phase at 87 vol.%, pigeonite being the second most abundant phase at 9.8 vol.%, followed by 2.4 vol.% olivine (Fig. 2). Throughout the section, there are areas that are 100% maskelynite and completely crystal-free. No relict plagioclase boundaries are observed. Other areas, highlighted in Fig. 2C, D, contain up to ~17% of pyroxene and olivine. Ti-rich chromite and troilite are the most abundant minor phases (~0.3% and 0.1% respectively). Ilmenite, taenite and Ni-Fe sulfides are very rare at <0.01% each. Consistent with previous studies of NWA 3163 (and PS), no phosphate phases were detected (Connolly et al., 2006, 2008).

### 2.2. Shock history

In NWA 3163 most plagioclase is transformed to the optically isotropic maskelynite, and several areas maintain remnant birefringence. Such a feature is typical for rocks shocked to pressures where plagioclase starts to be

transformed into maskelynite. Maskelynite typically shows a smooth appearance due to the absence of cleavage planes, intragranular cracks and vesicles (Stöffler et al., 1986; Chen and El Goresy, 2000; Fritz et al., 2005a). Many of the fractures in pyroxene and olivine terminate at grain boundaries and are not filled with maskelynite. The contact between maskelynite and the enclosed olivine and pyroxene grains is sharp and not blurred by element diffusion (Bloch and Ganguly, 2014). In the studied NWA 3163 chip, relict plagioclase grain boundaries are absent. This is also observed in NWA 4881 and hence is a feature that likely relates to the processes associated with production of this lunar granulite and not the formation of maskelynite.

Occasionally, feldspathic shock melt veins are observed exhibiting flow textures in the glass which sometime hosts ~1 μm sized crystals. These crystals likely formed during cooling of the melt, and not by devitrification during a later annealing event. Pyroxene crystals in contact with this hot Ca-rich plagioclase melt were subject to eutectic melting as indicated by the chemically distinct halos and schlieren features around pyroxene crystals (see Supplementary Information for additional BSE images showing the characteristic features of NWA 3163).

The conversion of plagioclase to maskelynite provides constraints on the peak shock pressure (see Supplementary Information; Stöffler et al., 1986; Fritz et al., 2005b; Fernandes et al., 2010). At 20–24 GPa, Ca-rich plagioclase ($An_{94}$) undergoes a solid-state transformation to diaplectic glass (maskelynite; Fritz et al., 2011). At shock pressures above ~45 GPa, plagioclase melts and forms a glass with density and refractive indices like those of thermally produced glasses (Stöffler et al., 1986). An anorthositic rock shocked to 20–24 GPa has a post shock temperature increase of <200 °C. The method to calculate the post shock temperature is explained by Artemieva and Ivanov (2004) and Fritz et al. (2005b) and is graphically displayed for an anorthositic rock in the supporting online material of Fernandes et al. (2013). This shock induced maskelynization of plagioclase and temperature increase is not severe enough to affect the $^{40}Ar$–$^{39}Ar$ chronology of lunar rocks (see later; Deutsch and Scharer, 1994; Fernandes et al., 2009a, 2010). Especially if the shock induced maskelynitisation occurred during impact ejection from the Moon into space (Rubin, 2015), i.e., as a decimeter sized rock fragment that cools within several tens of minutes (Fritz et al., 2005b). Additional study of the melt veins and the maskelynite in the NWA 3163 chip was carried out by Raman Spectroscopy. The results of this are provided in the Supplementary Information (SI 2).

The petrographic features described above indicate a potential sequence of events as follows: (1) The thermal metamorphism that led to the formation of the lunar granulites due to a prolonged heating episode would have induced devitrification and occurred prior to the formation of maskelynite; (2) this was then followed by later impacts including the one that induced maskelynization. The shock deformation of plagioclase to maskelynite and the melt veins observed in NWA 3163, and the fall paired NWA 4881, could be related to the last shock event that ejected this rock from the Moon (see also Rubin, 2015).

## 3. ANALYTICAL METHODS

Electron probe microanalysis (EPMA) and *in situ* laser ablation inductively coupled plasma-mass spectrometry (LA-ICPMS) were performed on a polished slab of NWA 3163. Major and minor element concentrations were measured by EPMA with a Cameca SX100 at NASA-Johnson Space Center (NASA-JSC). Beam conditions of 15 kV and 20 nA were used for all phases. All standardization was performed using well-characterized natural mineral samples: orthoclase for K, oligoclase for Al and Na, olivine for Fe, diopside for Si, Mg, and Ca, chromite for Cr, apatite for P, troilite for S, rutile for Ti, and rhodonite for Mn. For maskelynite analysis, Si and Ca were calibrated against a natural plagioclase standard instead of diopside. Na was measured first in order to minimize loss by volatilization. Back-scattered electron (BSE) images of the polished slab were acquired with the electron probe and by a JEOL 5910LV scanning electron microscope (SEM), also located at NASA-JSC, at an accelerating voltage of 15 kV.

Trace element concentrations were measured by LA-ICPMS at the University of Houston (UH) using a CETAC LSX-213 solid-state Nd-YAG laser or a PhotonMachines Analyte193 ArF excimer laser paired with a Varian 810-MS quadrupole ICPMS. In both cases, a He carrier gas was used to transport the ablated material to the ICP-MS. For each analyzed spot (25 μm), a 10–15 s gas blank was collected prior to ~30 s of sample ablation. Laser ablation spots were chosen to be coincident with previous EPMA analyses. However, due to the generally homogeneous composition of the major mineral phases, particularly maskelynite, several laser ablation spots were in areas not previously analyzed by EPMA. All analyses avoided proximity to fractures in mineral grains in order to avoid the potential for contamination by calcite. Laser ablation data was reduced using Mg, Ca, and Ti as internal standards for olivine and pyroxene, plagioclase, and oxides, respectively. The United States Geological Survey (USGS) standard reference material BHVO-2G glass was used to correct for instrumental fractionation and drift using the commercial data reduction software package Glitter (http://www.glitter-gemoc.com). The USGS SRM BIR-1G glass was used to monitor external reproducibility.

A small fragment of NWA 3163 was crushed for Rb–Sr and Sm–Nd isotopic analyses. This stone is too fine grained to allow for traditional mineral picking: mineral clasts <200 μm, matrix grains predominantly <50 μm. Instead, 0.5–2 mm-sized fractions based on color index were separated (lights, intermediates, darks). All fractions were leached in 2.5 N HCl prior to dissolution. Samples were spiked with a mixed Rb–Sr and a mixed Sm–Nd spike. Each sample was dissolved in HF-$HNO_3$ followed by repeat dissolution in 6 N HCl. Samples were loaded into AG 50 × 8 100–200 μm cation exchange resin columns from which Rb, Sr and the REE's were collected separately. Rubidium was further purified on a second cation exchange column. Strontium was purified using Eichrom Sr-spec resin following the procedure outlined in Charlier et al. (2006). Rare earth element (REE) fractions were taken up in dilute HCl and passed through the Eichrom LN-spec

resin columns from which Nd and Sm were collected. For Sm–Nd, a second small fragment was crushed and separated (lights, intermediates, darks, pyroxene-rich) in order to improve the precision and accuracy of the initial Sm and Nd dataset. Additional information regarding the preparation of samples for isotopic analysis is provided in the Supplementary Information (SI 3).

Aliquots for Rb isotope analysis were loaded in 6 N HCl onto single Ta filaments and analyzed by Thermal Ionization Mass Spectrometry (TIMS) on a ThermoScientific Triton Plus instrument at UH. The weighted average $^{87}Rb/^{85}Rb$ of five analyses of PlamaCal Rb solution was $0.3856 \pm 0.0002$ ($2\sigma$) on 10–40 ng loads. Aliquots for Sr isotope analysis were loaded in $HNO_3$ onto single Re filaments using a TaF activator and analyzed by TIMS at UH. Repeat analysis of the NBS987 standard yielded $^{87}Sr/^{86}Sr$ of $0.710212 \pm 0.000011$ ($2\sigma$, $n = 3$). $^{87}Sr/^{86}Sr$ and $^{84}Sr/^{86}Sr$ ratios were corrected for mass fractionation using an exponential law and an $^{86}Sr/^{88}Sr$ ratio of 0.1194 All Sr-isotopic data throughout this work is reported to relative to the NBS987 standard value of 0.71024 (Thirlwall, 1991). Total procedural blanks for Rb and Sr were <60 pg and <100 pg respectively. Aliquots for Sm and Nd isotope analysis were loaded in 0.7 M $H_3PO_4$ onto Re filaments using a double filament configuration, one for ionization and one for sample evaporation and analyzed by TIMS at UH. Repeat analysis of the internal Ames standard yielded $^{143}Nd/^{144}Nd$ of $0.511887 \pm 0.000007$ ($2\sigma$, $n = 6$). Analysis of the LaJolla standard yielded $^{143}Nd/^{144}Nd$ of $0.511845 \pm 0.000005$. Neodymium isotopic ratios were corrected for mass fractionation using the exponential law with $^{146}Nd/^{144}Nd = 0.7219$. For Sm isotope analysis, repeat analysis of the Ames standard yielded $^{149}Sm/^{152}Sm$ of $0.516864 \pm 0.000005$ ($2\sigma$, $n = 4$). Samarium isotopes were corrected for mass fractionation using the exponential law with $^{147}Sm/^{152}Sm = 0.560828$. Total procedural blanks for Sm and Nd were <50 pg and <80 pg respectively.

For $^{40}Ar/^{39}Ar$ radioisotopic dating, infra-red laser step heating measurements were carried out at the Berkeley Geochronology Center, California. Prior to analyses, two bulk aliquots of NWA 4881 (aliquot 1 = 4.03 mg, and aliquot 2 = 3.11 mg) were irradiated for 100 h in a Cd-shielded (to minimize undesirable isotopic interference reactions) CLICIT facility of the TRIGA reactor at Oregon State University, USA. Samples and the neutron fluence monitor PP-20 hornblende (the same as Hb3gr) were loaded into pits within aluminum disks. A J-value of $0.026665 \pm 0.000126$ was calculated relative to an age of Hb3gr = $1073.6 \pm 0.046$ Ga (Schwarz and Trieloff, 2007) using $^{40}K$-decay constant of Schwarz et al. (2011). Ages calculated with this $^{40}K$-decay constant are, within error, the same as those calculated using the Renne et al. (2011) value for the $^{40}K$-decay constant. Correction factors for interfering isotopes correspond to the weighted mean of 10 years of measurements of K–Fe and $CaSi_2$ glasses and $CaF_2$ fluorite in the TRIGA reactor: $(^{39}Ar/^{37}Ar)_{Ca} = (7.60 \pm 0.09) \times 10^{-4}$, $(^{36}Ar/^{37}Ar)_{Ca} = (2.70 \pm 0.02) \times 10^{-4}$ and $(^{40}Ar/^{39}Ar)_K = (7.30 \pm 0.90) \times 10^{-4}$. The two aliquots were degassed separately using a defocused $CO_2$ laser. The gas was purified in a stainless steel extraction line using two C-50 getters and a cryogenic condensation trap. Ar-isotopes were measured in static mode using a MAP 215–50 mass spectrometer with a Balzers electron multiplier, mostly using 10 cycles of peak-hopping. A detailed description of the mass spectrometer and extraction line is given by Renne et al. (1998). Blank measurements were obtained after every three sample runs. Ar-isotopic data are corrected for blank, mass discrimination and radioactive decay. Further details for data reduction procedures are given in Burgess and Turner (1998), Renne et al. (1998), Fernandes et al. (2000, 2003), and Fernandes and Burgess (2005).

## 4. RESULTS

### 4.1. Bulk rock chemistry

A modal recombination approach was used to determine the bulk rock composition using the bulk modal estimates from Connolly et al. (2006) as these are likely more representative of bulk modal proportions than the NWA 3163 chip studied here, which contains a relatively high proportion of maskelynite (Fig. 2). The reconstructed bulk rock major and trace element concentrations of NWA 3163 is presented in Table 1. With respect to major elements, NWA 3163 has a bulk molar Mg/(Mg + Fe) of 0.61 and using these geochemical parameters, it can be classified as a ferroan granulitic breccia along with paired stone NWA 4881 (Fig. 1B, after Hudgins et al., 2011a,b). The majority of Apollo granulitic breccias are more magnesian with MgO/FeO > 1.0 but exhibit variable wt.% $Al_2O_3$ (21.3–33.9). The bulk composition of the majority of all granulitic breccias shown in Fig. 1B is relatively magnesian when compared to the bulk composition of the upper few kilometers of the feldspathic lunar crust: MgO/FeO > 0.8 (bulk estimate from Jolliff et al. 2006). Bulk wt.% $Al_2O_3$ for NWA 3163 and its paired stones ranges from 24.0 to 27.2 (this study; Fernandes et al., 2009b; Hudgins et al., 2011a,b). These high $Al_2O_3$ contents are consistent with ~75% plagioclase and indicate a plagioclase-rich protolith, potentially representing either a primary lunar highland lithology or a polymict precursor (Taylor, 2009). Fig. 3A compares chondrite-normalised REE plots for well-characterized lunar rock suites to those of NWA 3163. The NWA 3163 chondrite-normalised REE pattern is characterized by a positive Eu-anomaly: $Eu/Eu^* = 3.48$ (where $Eu/Eu^* = Eu_N/((Sm_N{}^*Gd_N)\text{^}0.5)$, and is REE-depleted by an order of magnitude in comparison to the Apollo granulites and noritic anorthosites (Fig. 3). It also lacks an obvious KREEP (lunar material rich in potassium [K], Rare Earth Elements [REE] and Phosphorus [P]) component and is distinct from the ITE-depleted ferroan anorthosites with a small HREE enrichment ($La_N/Lu_N$: 0.66; Fig. 3A). This is not observed in the data from Hudgins et al., 2011a,b and Fernandes et al. (2009a,b), which show slight LREE enrichment ($La_N/Lu_N = 1.01$ and 1.10 respectively, where $_N$ denotes normalization to chondrite, Fig. 3B). The NWA 3163 (PS) samples are distinct from the lunar FAS samples and characterized by a smaller Eu-anomaly and higher REE concentrations (Fig. 3B). Notably, NWA 3163 and 4881 are relatively

Table 1
Comparison of major and trace element concentrations for NWA 3163, NWA 4483, and NWA 4881.

| | NWA 3163 This work | NWA 3163 Hudgins et al. (2011a,b) | NWA 4483 INAA Hudgins et al. (2011a,b) | NWA 4881 INAA Hudgins et al. (2011a,b) | NWA 4881 EMP Fernandes et al. (2009a,b) | NWA 4881 XRF Fernandes et al. (2009a,b) | NWA 4881 INAA Fernandes et al. (2009a,b) |
|---|---|---|---|---|---|---|---|
| $SiO_2$ | 45.7 | 45.1 | | | 45.5 | 44.2 | |
| $TiO_2$ | 0.19 | 0.19 | | | 0.21 | 0.21 | |
| $Al_2O_3$ | 24 | 27.2 | | | 25.8 | 26.2 | |
| FeO | 8.48 | 5.84 | | | 6 | 5.67 | |
| MnO | 0.13 | 0.091 | | | 0.1 | 0.08 | |
| MgO | 7.44 | 5.01 | | | 5.86 | 4.43 | |
| CaO | 13.8 | 16.1 | | | 15.9 | 15.3 | |
| $Na_2O$ | 0.26 | 0.288 | | | 0.28 | – | |
| $K_2O$ | 0.02 | 0.023 | | | 0.03 | – | |
| $P_2O_5$ | 0.03 | 0.022 | | | 0.05 | 0.03 | |
| $Cr_2O_3$ | 0.09 | 0.15 | | | 0.19 | 0.13 | |
| Sc | 14.3 | 12.6 | 11.2 | 14.6 | | | 14.6 |
| Cr | 656 | 1025 | 889 | 1327 | | | |
| Co | 15.9 | 13.15 | 12.55 | 14.54 | | | 14.5 |
| Ni | 16 | 38 | 54 | 57 | | | $60 \pm 20$ |
| Sr | 122 | 137 | 143 | 138 | | | – |
| Zr | 10.1 | 16 | 13 | 15 | | | – |
| Ba | 13.7 | 17 | 40 | 86 | | | 86 |
| La | 0.64 | 0.791 | 0.921 | 0.914 | | | 0.91 |
| Ce | 1.69 | 2.17 | 2.48 | 2.47 | | | 2.5 |
| Nd | 1.17 | 1.6 | 1.6 | 0.9 | | | – |
| Sm | 0.4 | 0.489 | 0.526 | 0.526 | | | 0.53 |
| Eu | 0.56 | 0.658 | 0.682 | 0.638 | | | 0.64 |
| Tb | 0.12 | 0.123 | 0.129 | 0.126 | | | 0.13 |
| Yb | 0.62 | 0.548 | 0.57 | 0.587 | | | 0.59 |
| Lu | 0.1 | 0.081 | 0.084 | 0.086 | | | 0.086 |
| Hf | 0.3 | 0.33 | 0.34 | 0.33 | | | 0.33 |
| Ta | 0.02 | 0.043 | 0.045 | 0.029 | | | – |
| Ir | – | 1.8 | 1.5 | 2.3 | | | – |
| Au | – | 0.2 | 1.5 | 0.4 | | | – |
| Th | 0.04 | 0.099 | 0.118 | 0.107 | | | 0.11 |
| U | 0.02 | 0.04 | 0.03 | 0.06 | | | – |

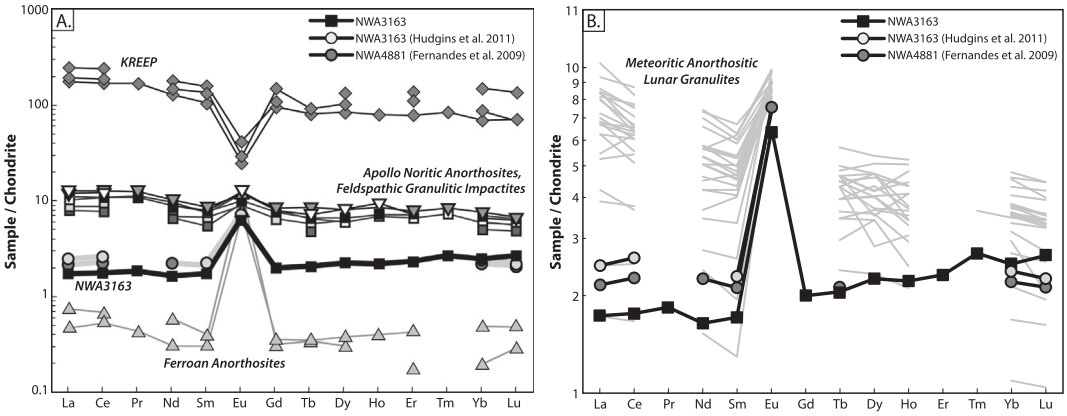


Fig. 3. (A) Bulk REE profiles of NWA 3163, 4881 compared to Apollo Granulites, Ferroan Anorthosites and KREEP samples. (B) REE profiles of NWA 3163, 4881 plotted alongside meteoritic anorthositic lunar granulites. Apollo granulites and impactites: 67016, 77017, 79215, 67415, 67955, 79215; Ferroan Anorthosites (FAS): 60025, 62236; KREEP: 12013, 14310, 15386; Meteoritic Anorthositic Lunar Granulites: NWA 5744, 482, ALHA 81005, QUE 93069, 94269, Y791197, 981031, DaG 025, 400, 262, Dho 026, 081, 457, 458, 459, 461, 462, 463, 464, 465, 466, 467, 468, 489. Data sources: Laul et al. (1983); Korotev et al. (2003), Warren (2005); Korotev et al. (2006); Lunar Sample Compendium, Meyer (2009); Fernandes et al. (2009a,b); Hudgins et al. (2011a,b).

LREE depleted in comparison to other anorthositic lunar granulites but exhibit similar LREE-MREE profiles (Fig. 3A).

Fig. 4 compares trace element concentrations of NWA 3163, 4881 and 4483 (measured by INAA, Hudgins et al., 2011a,b) to the trace element concentrations of NWA 3163 presented here (Table 1). There is a good 1:1 correlation between the data sets, with the main exceptions being Ba, Ni, and Th. Elevated Ba concentrations in NWA 4881 may reflect minor terrestrial contamination in the bulk rock powder used for INAA. The problems associated with estimating the overall percentage of metal and possible inhomogeneous distribution in a large sample could account for some of the discrepancy in plotted concentrations. Thorium is approximately a factor of two higher in NWA 4881 than in NWA 3163 (this study). The bulk analyses of NWA 3163 (PS) indicate that these meteorites are among the most trace element depleted lunar samples that have been studied to date (Fig. 3) and are notably more depleted than previously studies meteoritic anorthositic lunar granulites (Fig. 3B). From Fig. 3A, and consistent with previously studied Apollo noritic anorthosites and feldspathic granulitic impactites, NWA 3163 (PS) is relatively trace element-enriched compared to Ferroan Anorthosites (FANS) and is similar to 67215, a fragmental polymict breccia, sampled at North Ray Crater (Lindstrom and Salpas, 1983). Concentrations of Cr, Ti, and Ni are strongly influenced by the chosen modal proportion of oxides and preference should be given to true bulk rock analyses for these elements over what is presented here (Fernandes et al., 2009b; Hudgins et al., 2011a,b).

### 4.2. Major element mineral chemistry

The majority of pyroxene is low-Ca pigeonite at $Wo_{5\text{-}18}En_{53\text{-}61}Fs_{28\text{-}35}$ with an average of $Wo_{10}En_{57}Fs_{33}$. These compositions plot within a narrow range on the pyroxene composition quadrilateral (Fig. 5A, Table 2). Augite with $Wo_{26\text{-}38}En_{43\text{-}49}Fs_{18\text{-}25}$ and an average of $Wo_{33}En_{45}Fs_{21}$ is less common. Two slightly Fe-enriched pigeonite crystals ($Wo_{6.7}En_{53.8}Fs_{39.5}$) were also identified. Individual pyroxene crystals are unzoned and have, within error, homogeneous core to rim major element compositions. Mineral clasts of pyroxene have major element compositions indistinguishable from matrix pyroxene. Molar Fe/Mn ratios range from 42 to 69 with a mean of $56 \pm 12$ ($2\sigma$, all further errors $2\sigma$) excluding the several Fe-rich pigeonite crystals (Fe/Mn = 70–88). The Fe/Mn ratio of pyroxene in NWA 3163 is slightly lower than the lunar pyroxene Fe/Mn trend (66.7) of Papike et al. (2003). Pigeonite Mg# ranges from 57.8 to 66.4, average $= 63.8 \pm 1.1$, while augite is slightly higher and ranges from 65.5 to 70.3 (mean $= 67.9 \pm 1.4$).

There is little variation in the anorthite content of maskelynite throughout the slab studied here. Compositions cover a narrow range from $An_{94}$ to $An_{98,}$ with an average is $96.9 \pm 1.6$, $n = 134$ (Fig. 5B). Olivine is relatively iron-rich and exhibits very little variation in forsterite content (Fo%) with mean Fo% at $57.7 \pm 2.0$ (Fig 5B). One olivine crystal has a Fo% of $59.7 \pm 0.2$, which lies just outside of the $2\sigma$ variation of other analyzed olivine grains. Molar Fe/Mn ratio ranges from 79 to 113, with a mean of $94 \pm 16$ and is within the range reported for lunar samples (Papike et al., 2003: $103 \pm 20$). Spinel compositions have 53–82% chromite component along the chromite-ulvöspinel solid solution series $Fe_2TiO_4$–$FeCr_2O_4$. From the work of Hudgins et al., 2011a,b, the compositions of mineral clasts and matrix phases are indistinguishable, implying that the mineral clasts and their surrounding matrix are derived from a common progenitor. Two-pyroxene thermometry on co-existing orthopyroxene and augite yields an equilibrium temperature of 1070 °C, which is in good agreement with temperatures of 1096 °C estimated from pigeonite compositions using the calibration of Ishii (1975). From the Ca–Mg graphical thermometer shown in Fig. 5C, the majority of pyroxene yields temperatures between 1050 °C and 1100 °C (after Lindsley, 1983). These temperatures

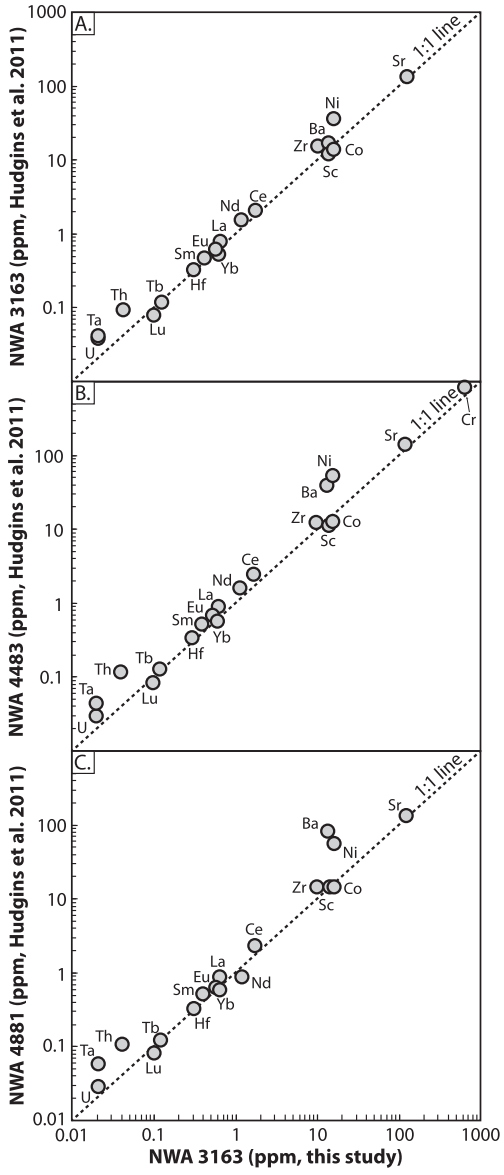


Fig. 4. Concentrations of trace elements (ppm) in NWA 3163 reconstructed bulk rock vs. concentrations of trace elements (ppm) in paired samples NWA 4483 and 4881. There is a general 1:1 correlation in concentrations with the exception of Ba, Ni, and Th. Reasons for these discrepancies are discussed in the text. Note: Each axis shows 5 orders of magnitude change in concentration.

are in excellent agreement with those reported by Hudgins et al., 2011a,b of 1050 ± 50 °C and are consistent with the two-pyroxene equilibration temperatures calculated for Apollo and Luna granulitic samples of 1100 ± 50 °C (Taylor, 2009).

### 4.3. Minor and trace element concentration of the main phases

Augite and pigeonite display similar chondrite-normalized profiles characterized by negative Sr and Eu anomalies (Fig. 6, Table 3). Plagioclase exhibits a characteristic positive Sr anomaly, which is mirrored in the bulk rock profile. Pyroxene is LREE depleted ($La/Yb_N = 0.08$) and the negative Eu anomalies ($Eu/Eu^* < 0.1$, Fig. 6B) imply that pyroxene crystallized from a Eu-depleted melt, i.e. during or after substantial plagioclase crystallization. Consistent with what is observed for olivine, there are no systematic differences in the trace element compositions between the larger pyroxene clasts and smaller groundmass pyroxene. Plagioclase exhibits a characteristic positive Eu anomaly ($Eu/Eu^* \sim 4$) typical of lunar plagioclase and has HREE depleted chondrite-normalized REE profiles ($La/Yb_N = 12.5$, Fig. 6). The chondrite-normalized profile of the calculated bulk rock is also shown in Fig. 6B, the main characteristics of which are mirrored by the signatures observed in plagioclase (positive Sr and Eu anomalies). This is consistent with NWA 3163 being dominated by plagioclase/maskelynite. The high Sr/Ba ratio of the plagioclase/maskelynite of 9.4, is also indicative of FAS-affinity in comparison to what would be expected from Mg-suite and KREEP samples (Norman et al., 2016).

### 4.4. Rb–Sr, Sm–Nd isotopic data

Pure mineral fractions could not be fully separated due to the fine-grained nature of NWA 3163 (Fig. 2). Instead, fractions were separated based on color index. For the first analytical campaign three fractions, lights, intermediates and darks (and a combined leachate) were obtained for Rb–Sr and Sm–Nd isotope analysis. A second analytical campaign targeted four fractions for additional Sm–Nd isotope analyses that included lights, intermediates, darks and a pyroxene-rich fraction (and four corresponding leachates), in an attempt to improve on the precision and accuracy of the Sm–Nd isotope data from the first campaign.

Results from Rb–Sr isotope analyses of NWA 3163 fractions are summarized in Table 4. The analyzed fractions do not plot on an isochron (Fig. 7). The measured $^{87}Sr/^{86}Sr$ of the three mineral fractions are identical within error and define an average value of 0.699282 ± 0.000007 (2σ). The measured $^{87}Sr/^{86}Sr$ for the leachate is 0.700690 ± 0.000011 (2σ). Strontium model ages are calculated using a present day $^{87}Sr/^{86}Sr$ Basaltic Achondrite Best Initial (BABI) present-day value of 0.70475, from initial $^{87}Sr/^{86}Sr$ value of 0.69891 (BABI) and a corresponding $^{87}Rb/^{86}Sr$ of 0.08716 (at 4.57 Ga after Podosek et al., 1991; Halliday and Porcelli, 2001). For all calculations, $\lambda^{87}Rb = 1.402 \times 10^{-11}$/yr based on Rb–Sr and U–Th–Pb systematics from chondritic meteorites (Minster et al., 1982; Snyder et al., 2000). A Sr model $T_{MA}$ age represents the time of separation of isolation of the source relative to an evolving chondrite reservoir and the sample Rb/Sr ratio is used to calculate the model age (Faure, 1986). A Sr model $T_{RD}$ age is a Rb depletion age and assumes no contribution from Rb in the sample in the age calculated (Faure, 1986, Table 4). The calculated source model Sr $T_{MA}$ age is 4.560 ± 0.012 Ga. The calculated source model Sr $T_{RD}$ age is 4.340 ± 0.006 Ga. The corresponding $^{87}Sr/^{86}Sr$ values for these ages are 0.699005 ± 0.000015 (2σ, $T_{MA}$) and 0.699015 ± 0.000015

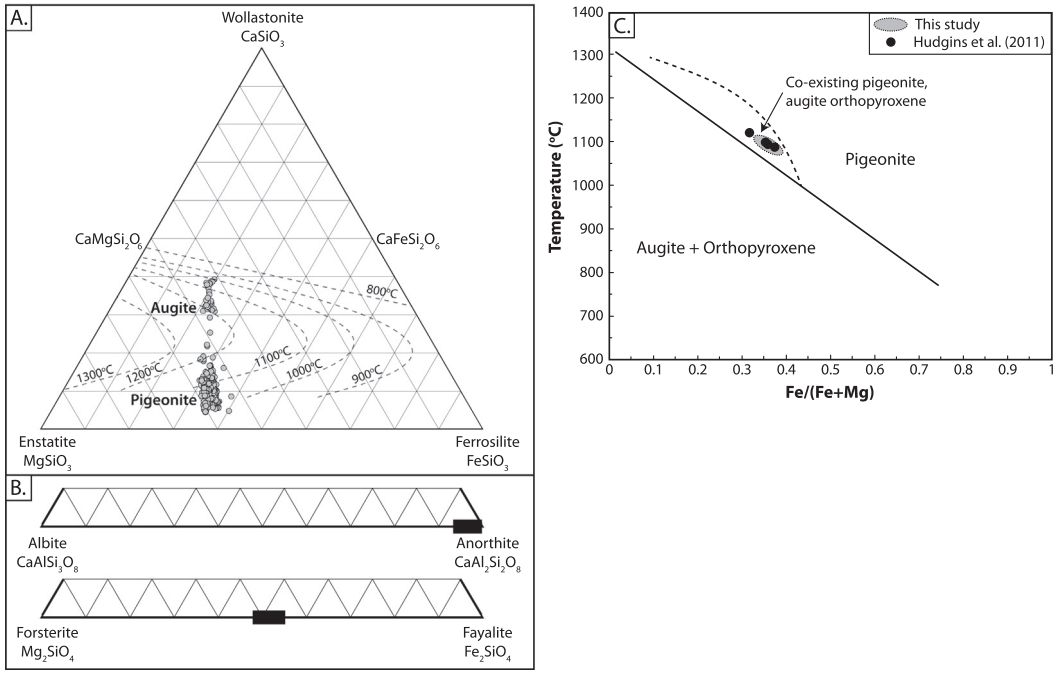


Fig. 5. (A) NWA 3163 pyroxene compositions plotted with the pyroxene thermometer after Lindsley (1983) at P <2 kb). (B) Compositions of plagioclase glass (maskelynite) and olivine in NWA3163. (C) Minimum crystallization temperatures calculated for NWA 3163 using the pigeonite thermometer of Ishii (1975).

(2σ, $T_{RD}$) respectively and are indistinguishable from each other.

From the first analytical campaign, measured $^{143}Nd/^{144}Nd$ for the intermediate fraction is 0.513082 ± 0.000010 (2σ) and for the dark fraction is 0.513567 ± 0.000011 (2σ). The combined leachates have measured $^{143}Nd/^{144}Nd$ of 0.511031 ± 0.000010 (2σ). No data are reported for the light fraction as a result of a relatively large blank correction applied to this fraction (23%) and poor signal intensity during TIMS analysis. For this reason a second analytical campaign targeting larger concentrations of Sm and Nd was undertaken. From this, the light fraction dominated by maskelynite is $^{143}Nd/^{144}Nd = 0.512776$ ± 0.000009 (2σ), compared to 0.512969 ± 0.000007 (2σ) for the pyroxene-rich fraction. Measured $^{143}Nd/^{144}Nd$ for the leachates, which were not combined, ranges from 0.510858 ± 0.000007 (2σ) for the intermediate fraction to 0.511280 ± 0.000010 (2σ) for the dark fraction. From the first campaign, $^{147}Sm/^{144}Nd$ ratios are 0.2139 ± 0.0011 (2σ) and 0.2306 ± 0.0012 (2σ) for the intermediate and dark fractions respectively. From the second campaign, the $^{147}Sm/^{144}Nd$ range is limited to 0.2036 ± 0.0010 (2σ) and 0.2070 ± 0.0010 (2σ) from analyses of the pyroxene-rich fraction and the dark fraction respectively. Considering data from both campaigns, and due to the limited range of Sm/Nd values, measured ratios define a scatterchron with a poorly defined date of *c.* 3.47 Ga with large errors (+290/−810 Ma), and the $^{143}Nd/^{144}Nd_i = 0.50826$ ± 0.00063 with $\varepsilon Nd_i = +1.0 \pm 3.6$ (Fig. 8A). Data from the second analytical campaign, where the leachates from each sample were not combined, are shown in Fig. 8B. The light, intermediate and pyroxene-rich fractions define sub parallel trends on Sm–Nd isotopic space with slopes = 0.0231–0.0241 and resulting dates from 3.64 Ga to 3.49 Ga (Fig. 8B). The dark fraction defines a slope of 0.0187 and a date of 2.83 Ga. Given the large uncertainty associated with the calculated $\varepsilon Nd_i$ and the scatterchron, no additional discussion of these data are presented as it does not add to the interpretation. The key conclusion is that Sm–Nd was reset during metamorphism and broadly agrees with ages from Ar–Ar dating (see below).

### 4.5. Ar–Ar dating of paired meteorite NWA 4881

The overall argon release pattern is comparable to that observed by Hudgins et al., 2011a,b for fractions of NWA 3163 and 4881 (Table 5, Fig. 9A). Both fragments in this study show similar release patterns; a total of 47–65 heating steps were obtained from Aliquots 1 and 2, respectively. The number of heating steps between analysis of Aliquot-1 and Aliquot-2 was increased in order to increase resolution of the data acquired. The Ar-release spectrum (Fig. 9A) for both aliquots is complex and indicates the implantation of excess $^{40}Ar$ in less retentive phases, followed by partial resetting with the higher temperatures revealing an older age. The initial ~17% to ~20% of gas release is dominated by implanted $^{40}Ar$ degassed by different domains within the sample. Evidence for this is provided by the rapid increase and decrease in apparent ages above the age of the Solar System. This release pattern is followed by a decline in apparent ages to a minimum of 1.98 ± 0.05 Ga, which presents a more recent event at ⩽2 Ga, which partially reset the K–Ar system (Aliquot-1). After this, there is a gradual increase in apparent ages.

Table 2
Average major element composition of major mineral phases.

| | Olivine $n = 51$ | 2σ | Pigeonite $n = 97$ | 2σ | Augite $n = 27$ | 2σ | Maskelynite $n = 134$ | 2σ | Chromite $n = 16$ | 2σ | Ilmenite $n = 10$ | 2σ | Reconstruced bulk rock |
|---|---|---|---|---|---|---|---|---|---|---|---|---|---|
| $SiO_2$ | 36.6 | 1.2 | 52.6 | 3 | 51.5 | 2.22 | 44.7 | 1.14 | 0.55 | 1.3 | 0.22 | 0.46 | 45.7 |
| $TiO_2$ | 0.06 | 0.06 | 0.69 | 0.52 | 1.09 | 0.86 | 0.03 | 0.1 | 19.8 | 1 | 52 | 1.66 | 0.19 |
| $Al_2O_3$ | 0.5 | 1.72 | 1.27 | 1.44 | 2.21 | 1.56 | 35.3 | 3.8 | 5.47 | 0.8 | 0.29 | 0.6 | 24 |
| FeO | 34.8 | 2.2 | 20 | 2.8 | 13.1 | 3.2 | 0.55 | 3.2 | 48.1 | 2.4 | 41.7 | 0.82 | 8.48 |
| MnO | 0.37 | 0.06 | 0.36 | 0.08 | 0.24 | 0.08 | 0.01 | 0.04 | 0.32 | 0.08 | 0.41 | 0.06 | 0.13 |
| MgO | 26.7 | 2 | 19.8 | 1.58 | 15.5 | 2.2 | 0.33 | 2.6 | 2.84 | 0.76 | 3.62 | 0.14 | 7.44 |
| CaO | 0.3 | 0.66 | 4.93 | 2.96 | 15.4 | 5 | 18.9 | 1.98 | 0.25 | 0.22 | 0.36 | 0.38 | 13.8 |
| $Na_2O$ | 0.01 | 0.02 | 0.02 | 0.02 | 0.04 | 0.04 | 0.38 | 0.12 | 0.01 | 0.02 | 0.01 | 0.02 | 0.26 |
| $K_2O$ | 0.02 | 0.04 | 0.01 | 0.04 | 0.03 | 0.06 | 0.03 | 0.08 | 0.01 | 0.02 | 0.01 | 0.02 | 0.02 |
| $P_2O_5$ | 0.02 | 0.04 | 0.02 | 0.06 | 0.03 | 0.1 | 0.03 | 0.04 | 0.02 | 0.04 | 0.02 | 0.04 | 0.03 |
| $SO_2$ | 0.06 | 0.32 | 0.06 | 0.28 | 0.02 | 0.08 | 0.03 | 0.16 | 0.25 | 1.16 | 0.01 | 0.02 | 0.04 |
| $Cr_2O_3$ | 0.03 | 0.06 | 0.3 | 0.18 | 0.49 | 0.26 | 0.01 | 0.04 | 21.8 | 2 | 0.27 | 0.06 | 0.09 |
| NiO | 0.02 | 0.06 | 0.01 | 0.04 | 0.01 | 0.02 | 0.01 | 0.04 | 0.03 | 0.04 | | 0 | 0.01 |
| Total | 99.5 | 1.16 | 100 | 1.2 | 99.7 | 3.92 | 100.3 | 0.96 | 99.5 | 1.4 | 98.9 | 1.54 | 100.2 |
| Mg# | 57.7 | 1 | 63.8 | 1.1 | 67.9 | 1.4 | 38.1 | 12 | | | | | 61 |
| An | | | | | | | 96.9 | 0.81 | | | | | |
| En | | | 57.2 | 1.7 | 45.7 | 2.8 | | | | | | | |
| Fs | | | 32.5 | 1.8 | 21.7 | 2.4 | | | | | | | |
| Wo | | | 10.3 | 3.1 | 32.6 | 5.1 | | | | | | | |

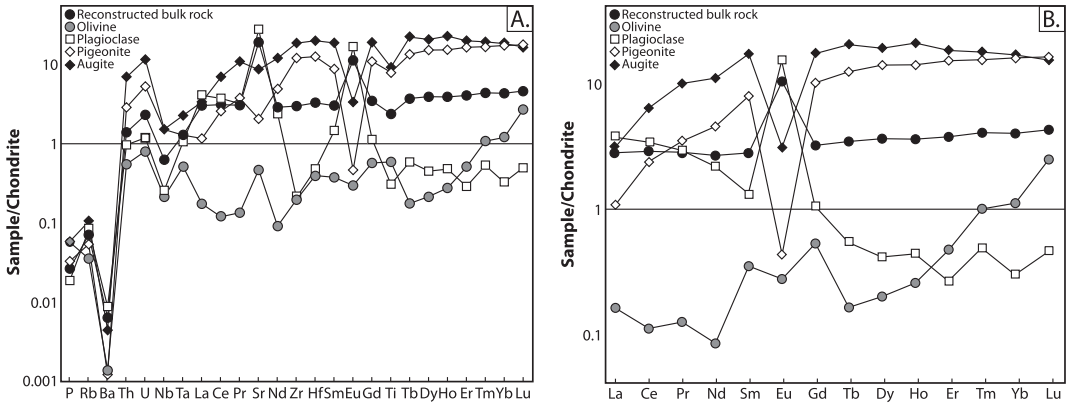


Fig. 6. (A) Chondrite normalized multi-element profiles of the main mineral phases in NWA 3163 and its reconstructed bulk rock composition based on observed mineral modes (Taylor and McCLennan, 1985). The positive Sr and Eu anomalies in the bulk rock are controlled by the abundance of plagioclase. (B) Chondrite normalized REE profiles for NWA 3163. Note the contrasting LREE depleted/HREE enriched pyroxene compositions and the LREE enriched/HREE depleted plagioclase composition. As these two phases are the dominant REE carrying phases in NWA 3163 (e.g., no phosphate was observed), the proportion of plagioclase to pyroxene controls the overall slope of the reconstructed bulk rock REE profile.

Table 3
Average trace element concentrations of major mineral phases (ppm).

| | Olivine $n=1$ | 1σ SD | Pigeonite $n=8$ | 1σ SD | Augite $n=4$ | 1σ SD | Maskelynite $n=12$ | 1σ SD | Chromite $n=6$ | Reconstruced bulk rock |
|---|---|---|---|---|---|---|---|---|---|---|
| P | 54.7 | 46.4 | 31.6 | 26.5 | 55.9 | 0.8 | 18.0 | 20.8 | 137.5 | 25.4 |
| Sc | 8.8 | 1.1 | 52.2 | 11.3 | 59.9 | 4.6 | 2.0 | 0.7 | 42.9 | 14.3 |
| Ti | 230.3 | 67.3 | 3114.8 | 647.0 | 3608.6 | 142.5 | 120.0 | 40.4 | | 930.0 |
| Cr | 143.4 | 33.6 | 2208.2 | 842.7 | 2634.7 | 495.5 | 10.1 | 10.6 | | 656.0 |
| Co | 80.4 | 6.6 | 32.3 | 6.4 | 39.4 | 12.2 | 0.5 | 2.0 | 131.8 | 15.9 |
| Ni | 56.3 | 11.2 | 8.8 | 13.4 | 17.0 | 8.2 | 12.0 | 22.3 | 221.7 | 16.0 |
| Zn | 26.3 | 4.4 | 18.5 | 4.2 | 19.0 | 3.5 | 0.7 | 0.3 | 325.0 | 7.5 |
| Ga | 0.1 | 0.0 | 0.3 | 0.2 | 0.5 | 0.4 | 3.2 | 0.5 | 17.8 | 2.2 |
| Ge | 1.0 | 0.6 | 0.7 | 0.6 | 1.7 | 1.7 | 0.7 | 0.4 | 3.8 | 0.8 |
| Rb | 0.1 | 0.1 | 0.1 | 0.0 | 0.2 | 0.2 | 0.2 | 0.1 | 0.4 | 0.1 |
| Sr | 7.7 | 2.7 | 13.3 | 6.2 | 55.4 | 53.0 | 176.8 | 10.6 | 43.4 | 122.0 |
| Y | 0.4 | 0.2 | 20.9 | 3.6 | 27.0 | 0.6 | 0.5 | 0.1 | 2.4 | 5.3 |
| Zr | 0.7 | 0.9 | 40.9 | 8.9 | 63.0 | 13.3 | 0.7 | 0.5 | 190.5 | 10.1 |
| Nb | 0.0 | 0.0 | 0.3 | 0.2 | 0.3 | 0.0 | 0.1 | 0.1 | 37.0 | 0.1 |
| Ba | 3.0 | 1.3 | 2.6 | 2.0 | 9.6 | 8.0 | 18.8 | 4.7 | 12.7 | 13.7 |
| La | 36.6 | 27.4 | 245.0 | 69.1 | 710.5 | 152.0 | 858.5 | 282.6 | 154.0 | 0.6 |
| Ce | 65.2 | 52.9 | 1402.0 | 370.5 | 3755.0 | 530.3 | 2030.0 | 530.2 | 520.0 | 1.7 |
| Pr | 11.1 | 4.2 | 309.0 | 79.6 | 893.0 | 199.4 | 264.2 | 69.5 | 116.0 | 0.3 |
| Nd | 37.0 | 21.5 | 1995.0 | 556.8 | 4855.0 | 374.8 | 969.0 | 284.8 | 504.0 | 1.2 |
| Sm | 49.5 | 32.8 | 1130.0 | 270.8 | 2455.0 | 346.5 | 190.5 | 72.3 | 142.0 | 0.4 |
| Eu | 14.9 | 11.5 | 23.3 | 23.6 | 167.8 | 192.6 | 829.5 | 58.7 | 66.0 | 0.6 |
| Gd | 101.0 | 111.1 | 1940.0 | 402.2 | 3320.0 | 56.6 | 203.0 | 84.7 | 830.0 | 0.6 |
| Tb | 5.7 | 4.2 | 431.0 | 84.1 | 709.5 | 17.7 | 18.9 | 11.0 | 68.0 | 0.1 |
| Dy | 47.0 | 29.2 | 3320.0 | 607.4 | 4525.0 | 459.6 | 98.5 | 35.7 | 467.0 | 0.9 |
| Ho | 13.4 | 7.5 | 741.0 | 120.2 | 1105.0 | 49.5 | 23.2 | 30.4 | 45.0 | 0.2 |
| Er | 72.0 | 24.8 | 2340.0 | 392.3 | 2825.0 | 91.9 | 41.1 | 52.3 | 215.0 | 0.6 |
| Tm | 23.7 | 10.1 | 368.0 | 73.6 | 423.5 | 51.6 | 11.7 | 10.2 | 20.6 | 0.1 |
| Yb | 171.5 | 43.0 | 2482.0 | 463.0 | 2620.0 | 396.0 | 46.5 | 22.5 | 270.0 | 0.6 |
| Lu | 58.4 | 22.8 | 386.0 | 69.6 | 364.0 | 17.0 | 10.9 | 18.5 | 50.0 | 0.1 |
| Hf | 36.3 | 33.0 | 1150.0 | 321.1 | 1825.0 | 49.5 | 43.5 | 40.8 | 5090.0 | 0.3 |
| Ta | 6.2 | 1.9 | 15.5 | 15.5 | 27.5 | 8.3 | 12.8 | 9.0 | 3430.0 | 0.0 |
| Th | 14.2 | 33.4 | 74.0 | 41.5 | 178.0 | 21.2 | 24.9 | 34.6 | 112.0 | 0.0 |
| U | 5.3 | 3.9 | 34.7 | 15.8 | 76.0 | 12.7 | 7.8 | 10.4 | 35.2 | 0.0 |

During the intermediate to high heating temperature steps, a total of ~50% of $^{39}Ar$ is released and there is a poorly defined plateau corresponding to an age of $3.17 \pm 0.20$ Ga and $3.52 \pm 0.11$ Ga for Aliquot-1 and Aliquot-2, respectively (average: $3.35 \pm 0.16$ Ga). This age is in agreement with Hudgins et al., 2011a,b who reported a mean age of

Table 4
Rb–Sr and Sm–Nd compositions for the measured light, intermediate and dark fractions and leachates for NWA 3163.

| Fraction | $^{87}Rb/^{86}Sr$ | | $^{87}Sr/^{86}Sr$ | 2σ | Rb (ppm) | Sr (ppm) |
|---|---|---|---|---|---|---|
| Lights | 0.00425 | 0.000021 | 0.699285 | 0.000013 | 0.05 | 36.2 |
| Intermediates | 0.00432 | 0.000022 | 0.699278 | 0.000007 | 0.13 | 85.7 |
| Darks | 0.00419 | 0.000021 | 0.699283 | 0.000006 | 0.07 | 49.2 |
| Leachate | 0.12512 | 0.000663 | 0.700690 | 0.000005 | 2.21 | 498 |
| Fraction | $^{147}Sm/^{144}Nd$ | | $^{143}Nd/^{144}Nd$ | 2σ | Sm (ppm) | Nd (ppm) |
| Lights | – | | – | | – | – |
| Intermediates | 0.21394 | 0.00107 | 0.513082 | 0.00106 | 0.37 | 1.02 |
| Darks | 0.23060 | 0.00115 | 0.513567 | 0.00115 | 0.27 | 0.67 |
| Leachate | 0.13796 | 0.00069 | 0.511031 | 0.00069 | 2.28 | 11.0 |
| Lights | 0.20618 | 0.00103 | 0.512776 | 0.000014 | 0.65 | 1.91 |
| Leachate | 0.12834 | 0.00064 | 0.510964 | 0.000010 | 0.38 | 1.81 |
| Intermediates | 0.20599 | 0.00103 | 0.512893 | 0.000004 | 0.49 | 1.45 |
| Leachate | 0.12154 | 0.00061 | 0.510858 | 0.000007 | 0.24 | 1.18 |
| Darks | 0.20699 | 0.00103 | 0.512894 | 0.000004 | 0.5 | 1.36 |
| Leachate | 0.12090 | 0.00060 | 0.511280 | 0.000010 | 0.32 | 1.61 |
| Pyx-rich | 0.20364 | 0.00102 | 0.512969 | 0.000006 | 0.54 | 2.78 |
| Leachate | 0.11676 | 0.00058 | 0.510958 | 0.000007 | 0.25 | 1.31 |

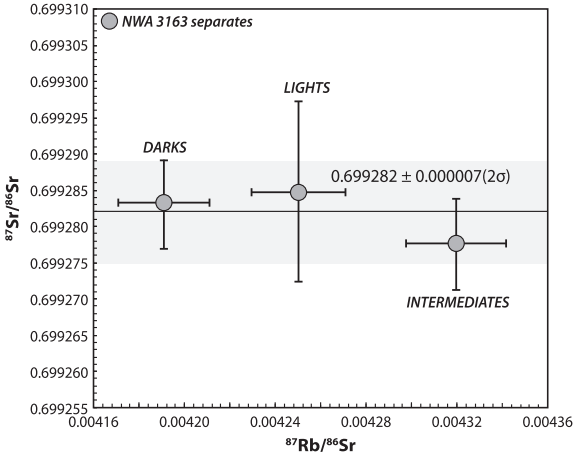


Fig. 7. Plot showing $^{87}Rb/^{86}Sr$ vs. $^{87}Sr/^{86}Sr$ for the dark, light and intermediate fractions of NWA 3163. The $^{87}Sr/^{86}Sr$ ratios are within error and are used to calculate Sr model ages. The leachate, at $^{87}Sr/^{86}Sr$: 0.70069 and $^{87}Rb/^{86}Sr$: 0.12512 is not shown.

$3.33 \pm 0.03$ Ga for NWA 3163. Using the recent updates on the $^{40}K$-decay constant (Renne et al., 2011; Schwarz et al., 2011) and sample-monitor age (Schwarz and Trieloff (2007), the Hudgins et al. (2011a,b) age for NWA 3163 of $3.33 \pm 0.03$ is corrected to $3.322 \pm 0.095$ Ga for NWA 3163. For NWA 4881, Hudgins et al. (2011a,b) reported a poorly defined age of $2.53 \pm 1.31$ Ga. Throughout Ar release, Ca/K ratios for both aliquots are ~1000, demonstrating a similar chemistry/mineralogy for both aliquots and indicative of a predominance of plagioclase.

The Ar data for each aliquot can be divided into two groups (Fig. 9B): (1) the low-temperature steps (the initial 17–20% of the $^{39}Ar$-release) which are dominated by a combination of trapped-excess-implanted and likely terrestrial $^{40}Ar$ with an initial $^{40}Ar/^{36}Ar$ of 305–325, a $^{38}Ar/^{36}Ar$ of ~0.1869, and a y-intercept (i.e., $^{40}Ar/^{39}Ar$) of a non-definable age and (2) the high-temperature steps characterized by $^{40}Ar/^{36}Ar$ values of ~218.4 and 184.4 for Aliquot-2 and Aliquot-1, respectively, representing a negligible variation in the $^{40}Ar/^{36}Ar$ suggesting no need to correct for trapped argon, and a $^{38}Ar/^{36}Ar$ of 1.2–1.5 indicating a predominance in cosmogenic Ar. From the $^{40}Ar/^{39}Ar$ of the intermediate and high temperature heating steps for each aliquot, ages of $3.474 \pm 0.036$ Ga and $3.216 \pm 0.080$ Ga for Aliquot-2 and Aliquot-1 respectively are calculated respectively. These ages are within error the same as those defined from the release spectra and reported above. The $^{38}Ar/^{36}Ar$ values for the intermediate and high temperature steps have increasing input from a cosmogenic component ($^{38}Ar/^{36}Ar = 1.54$) and less of the trapped component ($^{38}Ar/^{36}Ar = 0.1869$). No correction for solar wind was therefore made. Based on the method of Eugster and Michel (1995), a $2\pi$ $^{38}Ar$ production rate of $9.341 \times 10^{-9}$ cc/g/Ma was calculated which takes into account the $^{38}Ar$-contributions from the spallation of Ca, Fe, Ti, Cr, Mn, K, and Ni. For these calculations, the bulk chemical composition reported by Fernandes et al. (2009b) was applied. Using the measured $^{38}Ar$ and the calculated production rate, a cosmic ray exposure age of 22–25 Ma was calculated for NWA 4881. This is slightly older than that reported by Hudgins et al. (2011a,b) of 14.5 Ma for NWA 3163 and 16.0 Ma for NWA 4881. The difference can be attributed to slight differences in the mineralogical abundances between the different fragments used in the two studies and potentially differences in the $^{38}Ar$ production rate used.

The $^{39}Ar$–$^{40}Ar$ ages reported by this study for NWA 4881 and those from NWA 3163 reported in Hudgins et al. (2011a,b) are generally in good agreement. They suggest an earlier thermal event at *c.* 3.52 Ga which reset the Ar–Ar isotopic systematics. A more recent thermal event recorded by NWA 4881 at $\leqslant 2$ Ga (Fig. 9A) is not observed in NWA 3163. Both rocks show intermediate ages between 3.3 Ga and 2.8 Ga as evidence of this partial resetting of the

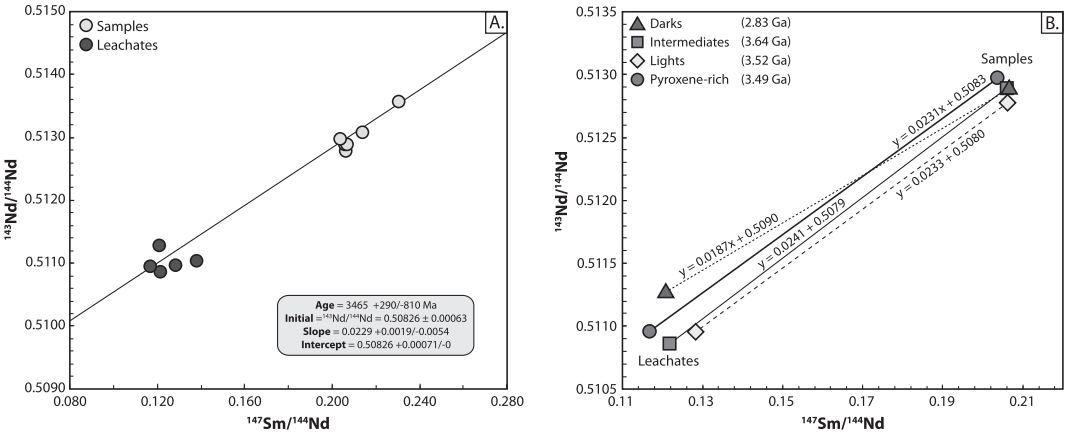


Fig. 8. (A) Graph showing results from Nd isotopic analyses of separated fractions of NWA 3163 from both analytical campaigns (data in Table 4). Considered together, the analyzed samples and leachates define a poorly defined scatterchron at $3.465^{+290}_{-810}$ Ga and $^{143}Nd/^{144}Nd_i = 0.50826$. Error bars at 2σ are smaller than symbol size. (B) Plot showing $^{147}Sm/^{144}Nd$ vs. $^{143}Nd/^{144}Nd$ for the separated fractions and their corresponding leachates from analytical campaign 2. Samples show little variation in $^{147}Sm/^{144}Nd$ and cluster at 0.205 ± 0.003.

Table 5
Results from Ar–Ar step heating of two bulk fragments of NWA 4881.

| Aliquot | Weight (mg) | Early event (Ga) | Late event (Ga) | CRE age (Ma) |
|---|---|---|---|---|
| 1 | 4.03 | 3.198 ± 0.026 | 2.744 ± 0.028 | 25 |
| 2 | 3.11 | 3.524 ± 0.112 | 1.953 ± 0.026 | 22 |

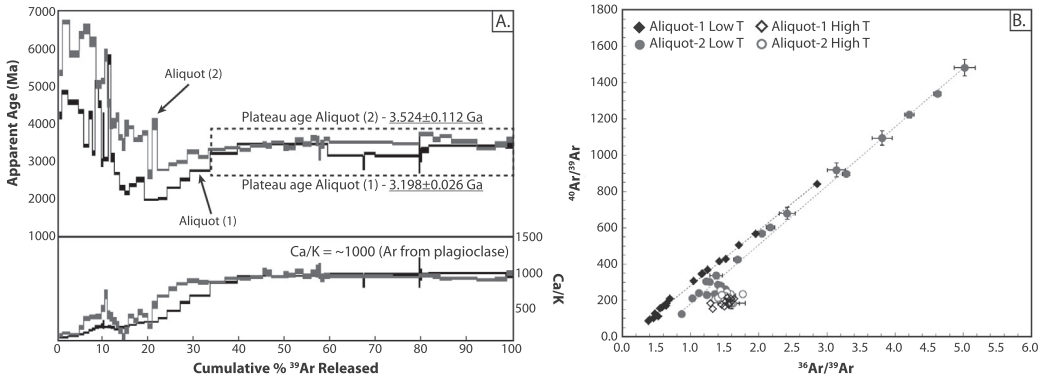


Fig. 9. (A) Ar–Ar step-heating release pattern for the two fragments of NWA 4881: top plot shows Apparent age vs. % $^{39}Ar$ released, and bottom plot shows Ca/K vs. % $^{39}Ar$ released. (B) Plot showing $^{40}Ar/^{39}Ar$ vs. $^{36}Ar/^{39}Ar$ where the *y*-axis is equivalent to age of the sample and the slope of the correlation line corresponds to the $^{40}Ar/^{36}Ar$.

K-Ar system, possibly due to differences in heating of the different portions of the parent rock. This could be attributed to heterogeneous heating throughout the sample (Hudgins et al., 2011a,b) as suggested by the partial resetting nature of this event.

## 5. DISCUSSION

### 5.1. Metamorphism of granulitic breccia NWA 3163 (PS)

The granulitic texture of the matrix of NWA (PS) indicates recrystallization by subsolidus heating of the protolith. Potential heat sources for the metamorphism include impact melt in the floors of small (30–90 km) or larger (100–200 km) craters, thick (2–5 km) superheated (>2000 °C) impact melt sheets, or proximal intrusions (Cushing et al., 1999; Korotev and Jolliff, 2001; Hudgins and Spray, 2009; Hudgins et al., 2011a,b). Previous work from Irving et al. (2006) suggests that the NWA 3163 granulitic breccia could have been produced through burial metamorphism of lunar crustal rocks that had been affected by impacts. The NWA 3163 (PS) have lower highly-siderophile elements (HSE) such as Ir and ITE concentrations than apparent near-surface regolith breccias and all other feldspathic lunar meteorites (Table 1, Korotev et al., 2003; Fernandes et al., 2009b; Hudgins et al.,

2011a,b). An increase in highly siderophile element and ITE concentrations in the lunar regolith could be expected over time due to micrometeorite impacts and global redistribution of ITE from the Procellarum KREEP Terrane (PKT), respectively (Korotev et al., 2003). This could result in mature regolith having high concentrations of both highly siderophile elements and ITE Korotev et al., 2003, 2006). Therefore, if NWA 3163 were a regolith breccia prior to heating, it may have been an immature one. These observations would be consistent with brecciation and thermal metamorphism of NWA 3163 likely occurring below the top layer of HSE contaminated regolith (~40 m, Wilcox et al., 2005) and probably below the upper <2 km of the lunar crust where (polymict) impact ejecta, and commingled melt sheets are present (Hiesinger and Head, 2006).

Another potential heat source would be magmatic intrusions that stall in the crust after reaching neutral buoyancy. The lunar farside is largely devoid of mare basalt flows and it has been hypothesized that this is a function of the thick and low-density crust in this region such that basaltic magmas are not buoyant enough to reach the surface (Solomon, 1975). If NWA (PS) 3163 originated on the lunar farside or far from the nearside Th-rich PKT (probable considering the low ITE concentrations), a ponded mare basalt intrusion could have provided the heat to achieve long-term subsolidus re-equilibration. However, this hypothesis is not consistent with the overall lack of 'mascons' (areas of high gravity on the lunar surface) in regions on the farside not associated with either large craters or the flooded crater floor of Moscoviense (Ghods and Arkani-Hamed, 2007; Laneuville et al., 2013). This implies a lack of ponded mare intrusions. This hypothesis, however, cannot be unequivocally ruled out as a small magma body could have ponded near the NWA (PS) 3163 protolith(s) creating a local thermal disturbance without creating an appreciable mascon, potentially during serial magmatism. The poikiloblastic texture of NWA (PS) 3163 (Fig. 2, Supplementary Figs. 1–4) is consistent with an impact (or a series of impacts) with induced melting as suggested for other lunar granulites (Cushing et al., 1999). Such impacts could potentially serve to brecciate and substantially excavate the protolith of NWA (PS) 3163 and provide the temperature increase and consequent thermal metamorphism (Hudgins et al., 2011a,b). In Supp. Fig. 3, fractures in the olivine and pyroxene are shown to be discontinuous and stop at clast boundaries with the matrix. They do not extend into the surrounding granulitic matrix thus implying that their poikiloblastic textures were produced during a different, earlier metamorphic event than the event that produced the granulitic texture of the matrix. This supports multiple episodes of impact-induced metamorphism during the petrogenesis of NWA 3163 (PS). This "serial impact" hypothesis is consistent with the multiple shock fractures present (Connolly et al., 2006) and the observation that maskelynization occurred after thermal metamorphism which itself was preceded by brecciation. An origin through serial impacts has also been proposed to explain magnesian granulitic breccias (Korotev and Jolliff, 2001) and may be the cause of brecciation, thermal metamorphism, and maskelynization for ferroan granulitic breccias as well, although Rubin (2015) proposed that maskelynization is most likely associated with an ejection event. From this, the metamorphism of the lunar crustal protoliths to NWA 3163 (PS) is inferred to be the result of an impact event.

- Two lines of arguments favor that maskelynitization occurred during a substantially younger impact event namely the impact that ejected the rock fragment from the lunar surface into space: Maskelynite in NWA 3163 and 4881 does not show cracks or fractures indicative for a shock event after the formation of smooth maskelynite.
- Rubin (2015) showed that the amount of strongly shocked rocks (containing maskelynite) from the lunar surface (i.e., Apollo samples) is rather small. In contrast many basaltic lunar meteorites contain maskelynite. This author argued that lunar meteorites provide random samples from the Moon but favors rocks that are shocked above a certain degree of shock pressure that achieved impact acceleration above escape velocity. This means that in most basaltic lunar meteorites the formation of maskelynite occurred during the impact ejection event (Rubin, 2015). The same observations and interpretation can be applied to the lunar granulitic breccias. The Apollo and Luna mission samples lack maskelynite but the lunar meteorites such as NWA 3163 and 4881 contain maskelynite. From this, it is thus likely the maskelynite observed in the meteorites formed during the ejection event.

From Hudgins et al. (2011a,b), and from several of the pyroxene grains observed in the sample NWA 3163 studied here, fine scale (<5 μm) exsolution lamellae were observed. From intraclast fracture patterns, these phases have previously been interpreted as relict phases which exsolved during slow cooling of the igneous protolith and therefore preserve information regarding the nature of the precursor lithologies to the NWA 3163 (PS) (Hudgins et al., 2011a,b). If phases in NWA 3163 (PS) represent primary crystallization from the LMO, then their trace element concentrations should be in equilibrium with residual LMO melts. Examination and further discussion of this potential origin is presented in the Supplementary Information (SI 4) in order to focus the remaining discussion on NWA 3163 (PS) within the context of the lunar (highlands) crust and subsequent lunar chronology.

### 5.2. NWA 3163 (PS) and the lunar highlands crust

One of the most fundamentally accepted concepts in lunar science is that the early Moon differentiated through crystallization of a LMO (Wood et al., 1970; Smith et al., 1970; Warren and Wasson, 1977; Warren, 1990). This led to the production of primordial lunar crust through plagioclase floatation and accumulation which today is inferred to be represented by the pristine FAN suite rocks composed of 96 vol% plagioclase on average (Carlson and Lugmair, 1988; Norman et al., 1995, 2003; Taylor, 2009; Nyquist et al., 2010). From near-infrared reflectance spectra, Hawke et al. (2003) reported that lunar anorthosites exist

at the near-surface below relatively mafic, pyroxene-rich layers within the shallow lunar crust. These plagioclase-rich layers were identified in the rings of prominent impact basins (Orientale, Nectaris and Nubium for example) and suggest that a global layer of anorthitic material may exist beneath the lunar surface. It is clear, however, that not all lunar anorthosites are direct products of LMO crystallization (e.g. James et al., 1989; Floss et al., 1998; Borg et al., 1999). From James et al. (1989), the FAS suite was subdivided into four groups: anorthositic ferroan (AF); mafic magnesian (MM); anorthositic sodic (AS) and mafic ferroan (MF). Only the AF and AS groups can be considered true, *sensu stricto*, FANs as they contain <10% mafic minerals. The FAS represent potential igneous precursors to the lunar granulites although it has been suggested that these subgroups do not share a common petrogenetic history (Floss et al., 1998). The NWA 3163 (PS) granulitic breccias can be classified as ferroan noritic anorthosites and are typically mineralogically and geochemically distinct from the FAS rocks: <90% plagioclase, high mafic phase component, MgO/FeO from 0.7 to 3.4, $Al_2O_3$ <30 wt.% and higher REE concentrations (Figs. 1 and 3). Despite these distinctions, the bulk composition of lunar granulites, including NWA 3163 (PS), overlap that of the average lunar highlands crust. For average lunar crust: FeO = 5.3–6.6 wt.%, $Al_2O_3$ = 24.6–26.1 wt.%, $SiO_2$ = 45.0–46.4 wt.% and CaO = 15.4–15.8 wt.% (values from Taylor, 1982; Palme et al., 1991). For comparison, average NWA 3163 (Table 1): FeO = 6.5 wt.% (±2.7, 2σ), $Al_2O_3$ = 25.8 wt.% (±2.7, 2σ), $SiO_2$ = 45.1 wt.% (±1.3, 2σ) and CaO = 15.3 wt.% (±2.1, 2σ), average from values shown in Table 1. It is worth noting that these bulk compositions are distinct from FAS rocks which exhibit $Al_2O_3$ typically >30% (Fig. 1B). These bulk values also overlap the bulk compositions reported for other lunar granulitic breccias: FeO = 5.6 wt.% (±2.9, 2σ), $Al_2O_3$ = 26.2 wt.% (±3.3, 2σ), and CaO = 15.2 wt.% (±1.5, 2σ), from samples 15418, 67215, 77017, 78155, 67415, 67955, 7630 and 79215 in Lindstrom and Lindstrom (1986, $SiO_2$ wt.% not reported; 67215 pertaining to the granular-textured clasts not the igneous-textured clast of Norman et al., 2003). Whilst pristine FAS samples may represent primary lunar crust (true FANs), which crystallized from a primordial (LMO), they are arguably not truly representative of the average lunar highlands crust. The bulk compositions of lunar granulites may therefore be more representative of the bulk lunar highlands crust as sampled today.

Lunar granulites clearly represent the reworking of pre-existing lunar lithologies and are often the product of impact melting and mixing. Recent studies on FAS samples support the idea that many FAS samples may also be the product of reworking and therefore not representative of direct crystallization products of a primary LMO (Boyet et al., 2014). Given the extensive impact history on the Moon, resurfacing, reworking and redistribution of primary igneous lithologies through repeated impact events has the potential to be a fundamental process through which the lunar crust, as sampled today, formed. This is supported by Norman et al. (1995), who in order to account for bulk crust Fe/Mg ratios, suggested that the contributions of the noritic anorthosites to the composition of the lunar crust has traditionally been overlooked. In order to balance the high $Al_2O_3$ contents of the plagioclase-rich ferroan anorthosites (>30 wt.%) with the bulk lunar crust (~25 wt.%), Warren and Kallemeyn (1993) suggested that Mg-suite magmatism following crystallization of a primary LMO contributed significantly to the lunar crust by up to 30 wt.% and that >20% of the lunar crust plagioclase is derived from post LMO magmatism. Mg-suite magmatism is understood to postdate (near) complete LMO solidification. The parental magmas to the Mg-suite may therefore have been derived from hybridization of KREEP-bearing lithologies and early-formed, plagioclase-dominated primary lunar crust (Gross et al., 2014; Shearer et al., 2015). This contribution from late Mg-suite magmatism provides a process through which primary anorthositic material could have been assimilated by later, more mafic melts and could provide, in part, a protolith component to NWA 3163 that would account for its relatively mafic nature:~5.8 wt.% FeO, ~5 wt.% MgO (Gross et al., 2014).

### 5.3. NWA 3163 (PS) and early lunar chronology

With respect to chronology, a wide range of ages characterizing the timing of crystallization of lunar samples is now available. From the LMO theory, samples of early-formed pristine lunar crust could provide constraints on the timing of LMO solidification. Boyet et al. (2014) recently argued that sample 62255 is the only true FAN sample to date to have been evaluated with respect to $^{142}Nd$. This sample yielded a crystallization age of 60–125 Myr after the onset of nebular condensation and was used to infer the timing of the Moon-forming giant impact. Other FAS samples previously dated in order to evaluate lunar crustal formation timescales, and previously argued to represent potentially primordial lunar crust range from 4.563 ± 0.120 Ga (Sm–Nd) to 4.290 ± 0.060 Ga (Sm–Nd), a time period of *c*. 270 Myr (Alibert et al., 1994; Borg et al., 1999). The implication from this could be that the LMO took *c*. 270 Myr to solidify.

Fig. 10 shows a compilation of FAS ages, $^{142}Nd$ model ages for the closure time of the Sm–Nd isotopic system in the mare basalt mantle source reservoirs, KREEP source model ages, the range of U–Pb ages in the lunar zircon record and the $T_{RD}$ Sr model age for NWA 3163 determined by this study at 4.340 ± 0.006 Ga. This age for NWA (PS) 3163 is consistent with previously determined model ages for the mare basalt source closure for the Sm–Nd isotopic system, which ranges from 4.355 + 0.031/−0.039 Ga to 4.320 + 0.030/−0.025 Ga (Nyquist et al., 1995; Rankenburg et al., 2006; Boyet and Carlson, 2007; Brandon et al., 2009; Gaffney and Borg 2014; McLeod et al., 2014) and KREEP model ages: 4.389 ± 0.045 Ga (Sm–Nd) and 4.353 ± 0.037 Ga (Lu–Hf) after Gaffney and Borg (2014). It should be noted, however, that the NWA 3163 Sr model age discussed here is a $T_{RD}$ age, i.e. a Rb depletion age and is taken as a minimum age constraint. This is therefore interpreted as a minimum age for the protolith to NWA 3163 and its paired stones 4881 and 4483. Nevertheless, this age is consistent with $^{142}Nd$

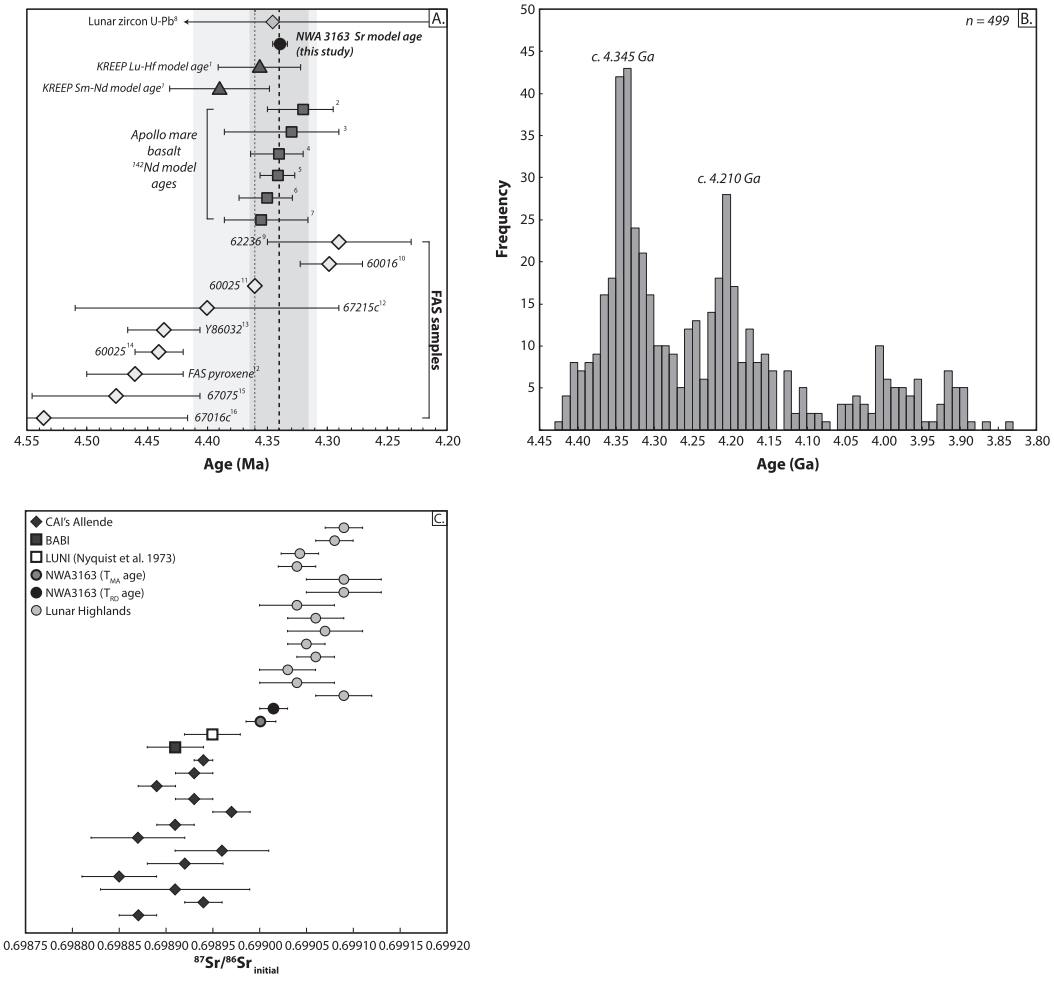


Fig. 10. (A) Graph summarizing current dates obtained on FAS samples, Apollo mare basalts, $^{142}$Nd model ages of FAS samples and Lu–Hf and Sm–Nd model ages of KREEP samples, compared to the $T_{RD}$ Sr model age of NWA 3163 from the present study. The thick black dashed line and accompanying grey shaded area (2σ) represents the average model age as defined six studies to date that have reported $^{142}$Nd data. The thin dashed line and accompanying grey shaded area (2σ) represents the average age defined by the KREEP model and the average $^{142}$Nd model age. NWA 3163 defines a $T_{RD}$ Sr model age of 4.339 ± 0.006 Ga (this study). KREEP model age data source: ages: Gaffney and Borg (2013)[1]. FAS data sources (Isotopic system in all cases is Sm–Nd): Carlson and Lugmair (1988)[14]; Alibert et al. (1994, recalculated in Borg et al., 1999)[16], Borg et al. (1999)[9]; Norman et al. (2003)[12]; Nyquist et al. (2006)[13]; Nyquist et al. (2010)[15]; Borg et al. (2011)[11]; Marks et al. (2014)[10]. $^{142}$Nd model age data sources: Nyquist et al. (1995)[3], Rankenburg et al. (2006)[6], Boyet and Carlson (2007)[2], Brandon et al. (2009)[4], Gaffney and Borg (2014)[7], McLeod et al. (2014)[5]. (B) Histogram showing U–Pb ages of lunar zircons from the Apollo 12, 14. 15 and 17 landing sites. Data sources[8]: Meyer et al. (1996); Pidgeon et al. (2007); Nemchin et al. (2008, 2009); Grange et al. (2009; 2011; 2013); Taylor (2009); Liu et al. (2012). (C) Graph showing $Sr_i$ compositions for NWA 3163 compared to those of Ca–Al inclusions (CAI) from carbonaceous chondrite Allende, of Lunar highland lithologies, BABI (Basaltic Achondrite Best Initial), and LUNI (Lunar Initial)): NWA 3163 $T_{MA}$ and $T_{RD}$ ages are 0.699005 ± 0.000015 and 0.699015 ± 0.000015 respectively. All data normalized to $^{87}Sr/^{86}Sr = 0.71024$ for NIST standard reference material 987. Data sources: Halliday and Porcelli (2001) and references therein.

model ages for mare basalts sources and KREEP model ages, and is close in age to the most precisely dated FAS sample to date, FAS 60025 at 4.360 ± 0.003 Ga (Fig. 10A, Borg et al., 2011). It should be noted that the young age for FAS 60025, relative to the previously reported age for that sample (Sm–Nd mineral isochron, Carlson and Lugmair, 1988, Fig. 10A), may not represent a primary igneous crystallization age as this lunar sample is polymict and consists of a number of different lithologies (Ryder, 1982; James et al., 1991; Warren and Taylor, 2013; Fernandes et al., 2013). Furthermore, a prominent age peak in the lunar zircon record at *c*. 4.345 Ga (Fig. 10B) from the Apollo 12, 14, 15 and 17 landing sites is also coincident with the NWA 3163 $T_{RD}$ Sr model age.

This lunar chronological history and the suite of young ages (⩽~4.35 Ga) emerging from lunar studies in recent years can be used to examine 3 scenarios for early lunar evolution (McLeod et al., 2014). In scenario 1, the Moon formed late at *c*. 4.35 Ga with a subsequent global LMO as inferred from the most recently published, relatively young FAS ages (Borg et al., 2011; Marks et al., 2014). In this scenario, the oldest reported FAS and U–Pb lunar

zircon ages would have to be erroneous (Fig. 10A, B). This interpretation also requires that the FAS rocks are differentiation products from a primary global LMO. In scenario 2, the Moon formed *c*. 70–110 Myr (4.50–4.45 Ga) after solar system formation as supported by U–Pb, Hf–W and Pu–I–Xe model ages, geodynamic *N*-body simulations and models of asteroidal meteorite impacts (Ozima and Podosek, 1999; Touboul et al., 2007; Halliday, 2008; Kleine et al., 2009; Jacobson et al., 2014; Bottke et al., 2015). This formation age is consistent with the range of ages exhibited by the lunar zircons that extend back in time beyond 4.35 Ga (Fig. 10B), and is in accordance with U–Pb and Hf isotopic constraints from the early Earth zircons (Harrison et al., 2008; Valley et al., 2014). The younger ages at *c*. 4.35 Ga, and therefore the model Sr $T_{RD}$ age for NWA 3163 (PS) at 4.34 Ga, would be interpreted as recording a later event in lunar evolution. In scenario 3, the Moon formed *c*. 70–110 Myr (as above) but the younger ages at *c*. 4.35 Ga record a prolonged crystallization history of the primordial LMO. This scenario remains to be comprehensively addressed. Current tidal heating models that propose to account for long LMO solidification timescales (Garrick-Bethell et al., 2010; Meyer et al., 2010) do not agree with petrological models. The latter require relatively short LMO crystallization timescales with 80% solidification after 1000 years, followed by 10 Myrs of subsequent solidification (Elkins-Tanton et al., 2011).

The calculated initial $^{87}Sr/^{86}Sr$ ratios for NWA 3163 of $0.699005 \pm 0.000015$ and $0.699015 \pm 0.000015$ ($2\sigma$) for the $T_{MA}$ and $T_{RD}$ Sr model ages, respectively, are plotted with $^{87}Sr/^{86}Sr_i$ values for lunar highland rocks and other Solar System reservoirs in Fig. 10C. It should be noted that the observed variability in Sr isotopes for early-formed planetary materials has been proposed as the result of nucleosynthetic anomalies and isotopic fractionation during the onset of nebular condensation (Papanastassiou and Wasserburg, 1978). With respect to materials from the Moon and Earth, however, a more recent study reported results from a $^{84}Sr$–$^{87}Sr$ double spike approach which demonstrated that samples define one mass dependent fractionation trend with respect to Sr isotopes (Charlier et al., 2014). As shown in Fig. 10C, all lunar samples have higher $^{87}Sr/^{86}Sr_i$, than earlier formed objects as would be expected for materials that formed later in solar system evolution with $^{87}Sr$ production from $^{87}Rb$ decay over time. All Calcium–Aluminum Inclusions (CAIs) plot within error of the BABI, which is thought to be the composition of the solar nebula at the time of early planetesimal formation; $^{87}Sr/^{86}Sr = 0.69891 \pm 0.00003$ (Fig. 10C). From this study, NWA 3163 overlaps within error, the $^{87}Sr/^{87}Sr_i$ range exhibited by lunar highland samples: of 0.69903–0.69909, with an average: $0.699062 \pm 0.000045$ ($n = 14$, $2\sigma$). All lunar highland samples, including NWA 3163, exhibit higher $^{87}Sr/^{86}Sr$ than the proposed lunar initial (LUNI after Nyquist, 1977b, Fig. 10C), with $^{87}Sr/^{86}Sr$ of $0.69895 \pm 0.00003$ at 4.55 Ga, likely indicating that the lunar highlands crust and NWA 3163 (PS) represent younger material with protracted $^{87}Rb$ decay relative to LUNI.

One of the ideas that emerges as a result of evaluating the geochemical and isotopic systematics of potentially primary igneous lunar crustal rocks within the context of the LMO, is that not all samples are direct LMO products but instead may represent the crystallization from early-formed fractionated melts, melts generated during late-stage reworking and/or resurfacing of early-formed lunar crust (Norman and Ryder, 1980; Arai et al., 2008). For example, (LMO) cumulate overturn (Elkins-Tanton et al., 2002; Zhang et al., 2013), serial magmatism (Borg et al., 2011) and late-stage crystallization of small volume residual LMO melts (Nemchin et al., 2009) have all been proposed as late stage mechanisms that could account for the observed range in lunar crustal ages.

### 5.4. NWA 3163 (PS) and the Moon's impact history

The NWA 3163 (PS) noritic anorthosite meteorites, and lunar granulitic breccias in general, are representative of the complex effects of impact bombardment on the lunar surface that led to metamorphism and produced the granulitic texture observed today (Fernandes et al., 2009b). The formation of impact craters and the subsequent effects of impact events have been key factors influencing the geochemical evolution of the Moon, in particular, the shallow crust (Warren and Taylor, 2013). Low concentrations of incompatible elements in NWA 3163 (PS; La = 0.64 ppm; Sm = 0.4 ppm, Ta = 0.02 ppm) indicate an origin distinct from the Procellarum KREEP Terrain. From 276 published $^{40}Ar/^{39}Ar$ impact ages to date from lunar meteorites and Apollo and Luna samples, a prominent peak at *c*. 3.95 Ga exists but resolvable peaks from 4.3 Ga to 0.25 Ga are also present (data compiled and presented in Fernandes et al., 2013). This wide age range potentially

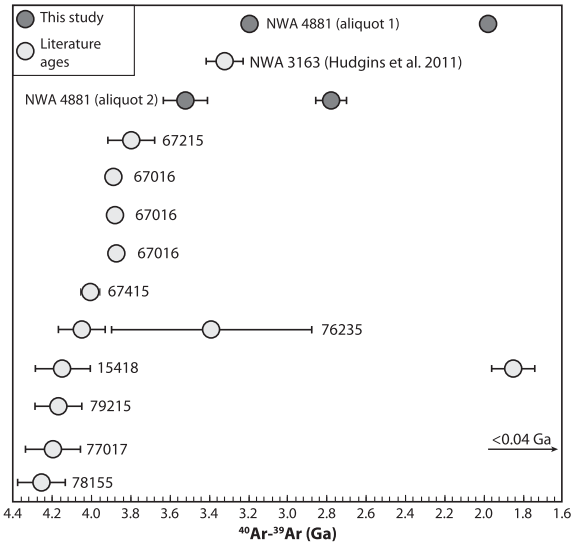


Fig. 11. Summary of Ar–Ar ages for lunar granulites plotted alongside results from NWA 4881 of this study. The Ar–Ar systematics of the Apollo samples have been corrected for the updated K-decay constant and the updated age-monitor age (Renne et al., 1998; 2010) Data sources: Stettler et al. (1973), Phinney et al. (1975), Turner and Cadogan (1975), Nunes et al. (1975), Cadogan and Turner (1976), McGee et al. (1978), Oberli et al. (1979), Marvin et al. (1987), Norman et al. (2010), Hudgins et al. (2008, 2011a,b), Schwarz et al. (2011), Fernandes et al. (2013).

indicates numerous impact events on the lunar surface and implies a complex bombardment history for the Moon. Impact ages from lunar meteorites broadly lie outside the range associated with returned Apollo and Luna samples at *c*. 4.1–3.8 Ga (Gomes et al., 2005), which may be the result of sampling bias (Schaeffer and Schaeffer, 1977; Norman et al., 2010; Fernandes et al., 2013). However, younger peaks within the Apollo collection have been identified and likely record younger impact events or periods of increased bombardment (*c*. 3.3 Ga, potentially between 1.8 and 2.2 Ga; Shuster et al., 2010, data reported and explained in Fernandes et al., 2013). A compilation of reported $^{40}Ar$–$^{39}Ar$ ages for lunar granulites is shown in Fig. 11. NWA 3163 and 4881 record the youngest cooling ages for lunar granulites (Hudgins et al., 2011a,b). For this reason, lunar meteorites such as NWA 3163 (PS) are invaluable as they are potentially derived from outside of landing site locations and provide additional constraints on the impact history of the lunar surface.

The reported $^{40}Ar$–$^{39}Ar$ data for NWA 4881 of this study suggests that the last thermal event this rock underwent, likely due to an impact has a maximum age of ~2 Ga. This age is consistent with the thermal event with a maximum age of 2.6 Ga and partial resetting between 2.0 and 2.5 Ga (or younger) reported by Hudgins et al. (2011a,b). This time correlates with a relative high impact flux onto the Moon between 1.8 and 2.2 Ga as inferred from lunar regolith samples (Fernandes et al., 2013). The older $^{40}Ar$–$^{39}Ar$ ages of $3.52 \pm 0.11$ Ga and $3.20 \pm 0.02$ Ga (average $3.35 \pm 0.20$ Ga) for NWA 4881 reported here for the high temperature heating steps are interpreted as a minimum age for the event that produced the granulitic nature of this breccia during which the K–Ar isotopic systematics were partially to totally reset. These results are consistent with the reported mean $^{40}Ar$–$^{39}Ar$ age of $3.327 \pm 0.029$ Ga from NWA 3163 and the indication of an age >3.0 Ga in NWA 4881 reported by Hudgins et al. (2011a,b). The *c*. 3.5 Ga date defined by the Sm–Nd scatterchron (Fig. 9A) is consistent with this result but whilst it potentially does provide supporting chronological evidence for an impact event at *c*. 3.5 Ga, it should be interpreted with caution. The age relies on the composition of the leachates being indigenous to the rock and not the result of terrestrial contamination. Nevertheless, three of the sample-leachate pairs define parallel slopes and similar dates (*c*. 3.5 Ga; Fig. 8B). The dark fraction, however, defines a much younger date at 2.83 Ga. Collectively, the leachate Sm–Nd isotopic signatures of the paired samples of NWA 3163 may therefore be interpreted as recording the closure age of the Sm–Nd system during the most recent thermal equilibration event. The paired sample-leachate Sm–Nd age is consistent with the Ar–Ar systematics at *c*. 3.5 Ga, a time interval towards the end of the intense lunar bombardment as testified by the crater populations on basaltic lunar surfaces with well-defined radiometric ages (Werner, 2014 and references therein). Alternatively, the poorly defined scatterchron data is the result of alteration with no chronological significance and the fact that it agrees with the Ar–Ar plateau age is a coincidence.

The chronology of NWA 3163 (PS) is summarized in Fig. 12 with respect to lunar evolution. From the minimum Sr $T_{RD}$ model age of 4.34 Ga to the $^{40}Ar$–$^{39}Ar$ age of ~2 Ga, these lunar granulitic breccias record a complex history of brecciation and metamorphism associated with crustal production and reworking during ~2.4 Gyrs of lunar history. From model ages and geodynamic models, the Moon formed 4.50–4.45 Ga following the Giant Impact (Fig. 12). During an intense period of lunar crustal reworking at *c*. 4.35 Ga, the protolith(s) to NWA 3163 (PS) likely formed as primary crustal lithologies were re-melted and metamorphosed, potentially as a result of a meteorite impact, density-driven cumulate overturn and/or serial magmatism (Fig. 12). Following this period of crustal reworking, the evolution of the lunar crust has since been predominantly influenced by the meteorite impacts, as recorded by the Ar–Ar systematics of lunar crustal rocks (see discussion above) and mare volcanism (Fig. 12). As samples of the lunar crust, the textural, mineralogical, geochemical and geochronological record of NWA 3163 (PS) imply that crustal production on the Moon is likely a multi-stage process involving several distinct lunar reservoirs.

## 6. CONCLUSIONS

The lunar granulitic breccia NWA 3163, and its paired stones 4881 and 4483, can be classified as a granulitic noritic anorthosite breccia and provides insights into the composition and complex metamorphic history of the Moon's anorthositic crust. The elevated Ni contents, and other siderophile elements, in NWA 3163 (PS) are characteristic of meteoritic contamination and combined with their granulitic nature, implies the role of an impact during their petrogenesis. From petrographic and textural observations, the thermal metamorphism of the NWA 3163 (PS) protolith(s) occurred prior to the formation of maskelynite as a prolonged heating would have led to plagioclase recrystallization. Following metamorphism of the lunar crustal protolith(s), maskelynization was induced by impacts. Two-pyroxene thermometry yields an equilibrium temperature of 1070 °C and from the Ca–Mg graphical thermometer, the majority of pyroxene yields temperatures between 1050 °C and 1100 °C. These temperatures are consistent with temperatures reported for Apollo and Luna granulitic samples ($1100 \pm 50$ °C).

Measured $^{87}Sr/^{86}Sr$ on bulk separates of NWA 3163 were indistinguishable with an average of $^{87}Sr/^{86}Sr = 0.699015 \pm 0.000015$. This value, and those of other lunar highland lithologies, $0.699062 \pm 0.000045$, $n = 14$, $2\sigma$, are distinct from the lunar initial of $0.69895 \pm 0.00003$ at 4.55 Ga (LUNI after Nyquist, 1977a,b). A model Sr $T_{RD}$ age, which is a minimum age, is calculated at *c*. 4.34 Ga for NWA 3163. Lunar highland lithologies like NWA 3163 therefore represent younger material compared to LUNI. Measured Sm–Nd isotopic systematics from bulk separates and associated leachates define a scatterchron with a date of *c*. 3.47 Ga. Consistent with this age are the Ar–Ar ages from two bulk separates of paired stone

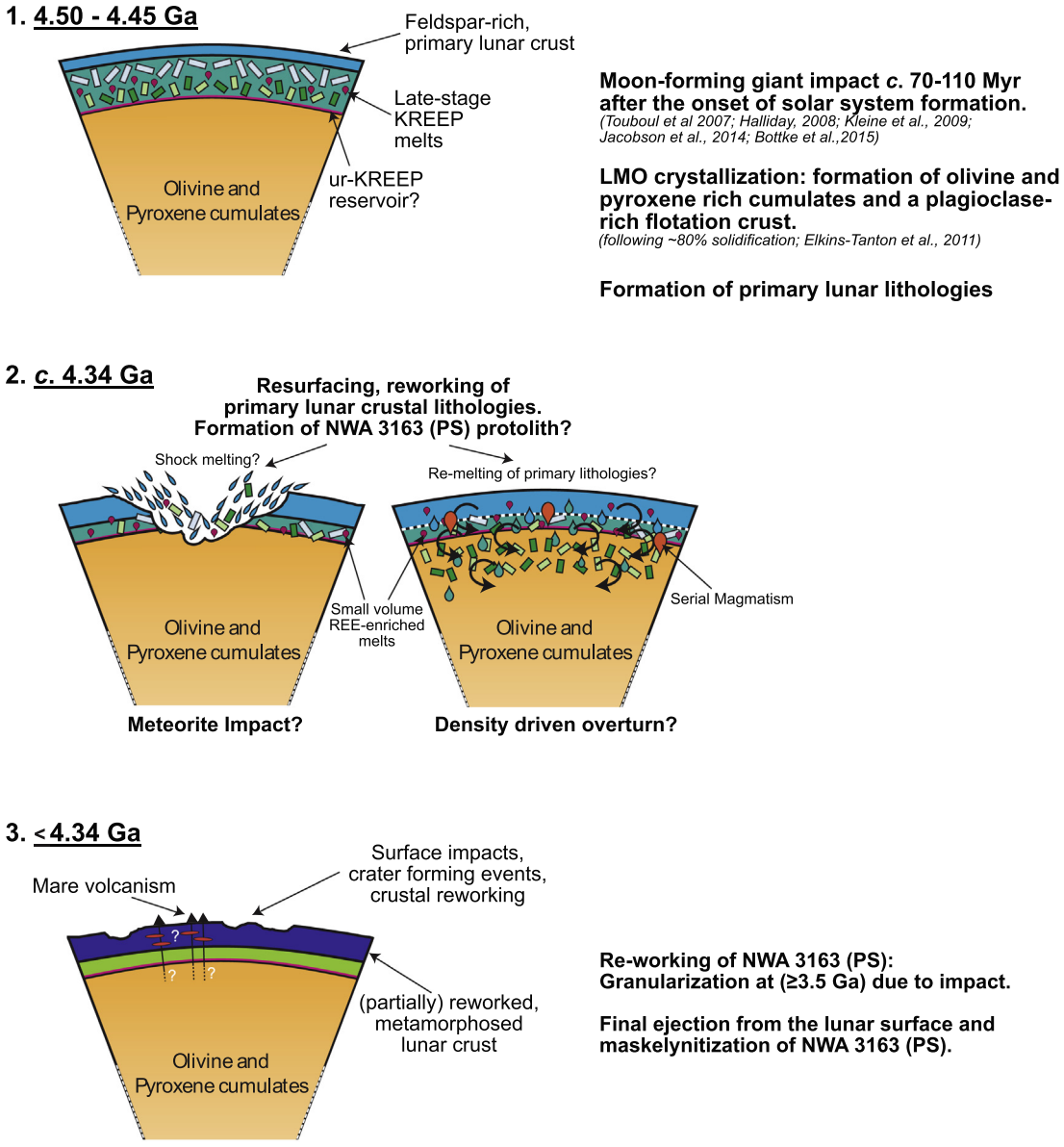


Fig. 12. Schematic summary showing the formation of NWA 3163 (PS) within the context of a primordial LMO c. 4.50 ± 0.06 Ga and reworking events subsequent to LMO crystallization. From the Sr $T_{RD}$ model age, the minimum age for the formation of the NWA 3163 (PS) protoliths is constrained to *c*. 4.34 Ga and is likely associated with significant lunar crustal reworking at this time. A major event on the Moon at this time is also supported by $^{142}$Nd model ages, the lunar zircon record, recently dated FAN samples, KREEP model ages (Fig. 10). Following this large, potentially Moon-wide event, the lunar surface continued to be reworked through the eruption of the mare basalts, meteorite impacts and subsequent crater formation. These later events led to the granularization of NWA 3163 (PS) at *c*. 3.4 Ga as constrained by Ar–Ar and hinted at by Sm–Nd (see text for discussion).

NWA 4881 which define plateau ages of 3.322 ± 0.095 Ga and 3.524 ± 0.112 Ga.

The model Sr $T_{RD}$ age of *c*. 4.34 Ga for NWA 3163 (PS) is within error of $^{142}$Nd model ages calculated from coupled $\mu^{142}$Nd-$\varepsilon^{143}$Nd systematics of the Apollo mare basalts: 4.355–4.314 Ga (Nyquist et al., 1995; Rankenburg et al., 2006; Boyet and Carlson, 2007; Brandon et al., 2009; Gaffney and Borg, 2014; McLeod et al., 2014). These Nd model ages have been interpreted as representing a resetting of isotopic systematics of the mare basalt source regions at this time. The Sr model age of *c*. 4.34 Ga would therefore be consistent with the lunar FAS samples not representing primary lunar crust but instead being products of remelting and subsequent re-crystallization of primary LMO differentiates. These age relationships also overlap with some recently reported young ages for the FAS suite; sample 60025: 4.360 ± 0.003 Ga and sample 60016: 4.290 + 0.024, −0.028 (Borg et al., 2011 and Marks et al., 2014

respectively), and a peak at 4.345 Ga for the U–Pb isotope ages of lunar zircons. Together, these age relationships indicate a major lunar event at *c*. 4.35 Ga that affected the upper mantle and crust. At this time, large scale reworking of preexisting crustal lithologies occurred and may have produced the protolith to the NWA 3163 (PS) ferroan granulitic breccias. The Ar–Ar isotopic systematics on aliquots of paired stone NWA 4881, and the Sm–Nd isotope systematics from NWA 3163, are consistent with an impact event at *c*. 3.4 Ga. This event is interpreted as an impact that induced metamorphism of the lunar crustal protoliths and produced the granulitic texture of the matrix. A later event at ~2 Ga as recorded by Ar–Ar is consistent with an increase in the number of impacts on the lunar surface at this time. Lunar granulitic breccias NWA 3163, 4881 and 4483 therefore record a *c*. 2.4 Gyr long history of lunar crustal formation, subsequent metamorphism of protolith material, brecciation, surface impact events and eventual ejection from the Moon.

## ACKNOWLEDGEMENTS

ADB received funding for this project through the Lunar Science Institute and the Cosmochemistry program at NASA. Gavyn Rollinson at the Camborne School of Mines, University of Exeter, UK is thanked for his assistance during acquisition of the QEMSCAN images. VAF acknowledges research funding from Deutsche Forshungsgeminschaft via grant FE 1523/3-1. Additional thanks are extended to 2 anonymous reviewers who comments and suggestions improved this manuscript. Further thanks to Marc Norman whose input significantly improved the discussion and interpretation of this new data.

## APPENDIX A. SUPPLEMENTARY DATA

Supplementary data associated with this article can be found, in the online version, at http://dx.doi.org/10.1016/j.gca.2016.04.032.

## REFERENCES

Alibert C., Norman M. D. and McCulloch M. T. (1994) An ancient age for a ferroan anorthosite clast from lunar breccia 67016. *Geochim. Cosmochim. Acta* **58**, 2921–2926.

Arai T., Takeda H., Yamaguchi A. and Ohtake M. (2008) A new model of lunar crust: asymmetry in crustal composition and evolution. *Earth Planets Space* **60**, 433–444.

Artemieva N. A. and Ivanov B. (2004) Launch of Martian meteorites in oblique impacts. *Icarus* **171**, 84–101.

Bloch E. and Ganguly J. (2014) $^{176}$Lu-$^{176}$Hf and $^{147}$Sm-$^{143}$Nd ages of the Martian shergottites: Evaluation of the shock-resetting hypothesis through diffusion kinetic experiments and modeling, and petrological observations. *Earth Planet. Sci. Lett.* **395**, 173–183.

Borg L., Norman M., Nyquist L., Bogard D., Snyder G., Taylor L. and Lindstrom M. (1999) Isotopic studies of ferroan anorthosite 62236: A young lunar crustal rock from a light rare-earth-element-depleted source. *Geochim. Cosmochim. Acta* **63**, 2679–2691.

Borg L., Connelly J., Boyet M. and Carlson R. W. (2011) Chronological evidence that the Moon is either young or did not have a global magma ocean. *Nature* **477**, 70–73.

Borg L. E., Gaffney A. M. and Shearer C. K. (2015) A review of lunar chronology revealing a preponderance of 4.34-4.37 Ga ages. *Meteorit. Planet. Sci.* **50**, 715–732.

Bottke W. F., Vokrouhlický S., Marchi S., Swindle T., Scott E. R. D., Weirich J. R. and Levison H. (2015) Dating the Moon-forming impact event with asteroidal meteorites. *Science* **348**, 321–324.

Boyet M. and Carlson R. W. (2007) A highly depleted Moon or a non-magma ocean origin for the lunar crust?. *Earth Planet. Sci. Lett.* **262** 505–516.

Boyet M., Carlson R. W., Borg L. E. and Horan M. (2014) Sm–Nd systematics of ferroan anorthositic suite rocks: Constraints on lunar crust formation. *Geochim. Cosmochim. Acta* **148**, 203–218.

Brandon A. D., Lapen T. J., Debaille V., Beard B. L., Rankenburg K. and Neal C. (2009) Re-evaluating $^{142}$Nd/$^{144}$Nd in lunar mare basalts with the implications for the early evolution and bulk Sm/Nd of the Moon. *Geochim. Cosmochim. Acta* **73**, 6421–6445.

Burgess R. and Turner G. (1998) Laser $^{40}$Ar–$^{39}$Ar age determinations of Luna 24 mare basalts. *Meteorit. Planet. Sci.* **33**, 921–935.

Cadogan P. H. and Turner G. (1976) The chronology of the Apollo 17 station 6 boulder. *Proceedings of Lunar Science Conference* **7**, 2267–2285.

Carlson R. W. and Lugmair G. W. (1988) The age of ferroan anorthosite: oldest crust on a young Moon? *Earth Planet. Sci. Lett.* **90**, 119–230.

Charlier B. L. A., Ginibre C., Morgan D., Nowell G. M., Pearson D. G., Davidson J. P. and Ottley C. J. (2006) Methods for the microsampling and high-precision analysis of strontium and rubidium isotopes at single crystal scale for petrological and geochronological applications. *Chem. Geol.* **232**, 114–133.

Charlier B., Parkinson I., Burton K. and Grady M. (2014). *Non-chondritic stable strontium ($\delta^{88}$Sr vs. $\delta^{84}$Sr) in the Earth, the Moon and some differentiated asteroids*, abstract; V13A–4719.

Chen M. and El Goresy A. (2000) The nature of maskelynite in shocked meteorites: not diaplectic glass but glass quenched from shock-induced dense melt at high pressures. *Earth Planet. Sci. Lett.* **179**, 489–502.

Cohen B. A., James O. B., Taylor L. A., Nazarov M. and Barsukova L. D. (2004) Lunar highland meteorite Dhofar 026 and Apollo sample 15418: Two strongly shocked, partially melted, granulitic breccias. *Meteorit. Planet. Sci.* **39**, 1419–1447.

Connolly H. C., Zipfel J., Grossman J. N., Folco L., Smith C., Jones R. H., Righter K., Zolensky M., Russell S. S., Benedix G. K., Yamaguchi A. and Cohen B. A. (2006) The meteoritcal bulletin, No. 90. *Meteorit. Planet. Sci.* **41**, 1383–1418.

Connolly H. C., Smith C., Benedix G., Folco L., Righter K., Zipfel J., Yamaguchi A. and Chennaoui Aoudjehane H. (2008) The meteoritcal bulletin, No. 93. *Meteorit. Planet. Sci.* **43**, 571–632.

Cushing J., Taylor G., Norman M. and Keil K. (1999) The granulitic impactite suite: Impact melts and metamorphic breccias of the early lunar crust. *Meteorit. Planet. Sci.* **34**, 185–195.

Demidova S. I., Nazarov M. A., Lorenz C. A., Kurat G., Brandstätter F. and Ntaflos Th. (2007) Chemical Composition of Lunar Meteorites and the Lunar Crust. *Petrologiya* **15**, 416–437.

Deutsch A. and Schärer U. (1994) Dating terrestrial impact events. *Meteoritics* **29**, 301–322.

Elkins-Tanton L. T., Van Orman J. A., Hager B. H. and Grove T. L. (2002) Re-examination of the lunar magma ocean cumulate overturn hypothesis: melting or mixing is required. *Earth Planet. Sci. Lett.* **196**, 239–249.

Elkins-Tanton L. T., Burgess S. and Yin Q.-Z. (2011) The lunar magma ocean: Reconciling the solidification process with lunar petrology and geochronology. *Earth Planet. Sci. Lett.* **304**, 326–336.

Eugster O. and Michel T. (1995) Common asteroid breakup events of eucrites, diogenites, and howardites, and cosmic ray production rates for noble gases in chondrites. *Geochim. Cosmochim. Acta* **59**, 177–199.

Faure G. (1986) *Principles of Isotope Geology*, second ed. Wiley Publishing, p. 608.

Fernandes V. A. and Burgess R. (2005) Volcanism in Mare Fecunditatis and Mare Crisium: Ar–Ar age studies. *Geochim. Cosmochim. Acta* **69**, 4919–4934.

Fernandes V. A., Burgess R. and Turner G. (2000) Laser $^{40}Ar/^{39}Ar$ age studies of Dar al Gani 262 Lunar meteorite. *Meteorit. Planet. Sci.* **35**, 1355–1364.

Fernandes V. A., Burgess R. and Turner G. (2003) Ar–Ar chronology of lunar meteorites Northwest Africa 032 and 773. *Meteorit. Planet. Sci.* **38**, 555–564.

Fernandes V. A., Burgess R. and Morris A. (2009a) 40Ar-39Ar age determinations of lunar basalt meteorites Asuka 881757, Yamato 793169, Miller Range 05035, LaPaz Icefield 02205, Northwest Africa 479, and basaltic breccia Elephant Moraine 96008. *Meteorit. Planet. Sci.* **44**, 805–821.

Fernandes V., Irving A., Kuehner S., Gellissen M., Korotev R. and Bandfield J. (2009b) Petrology, bulk composition, Ar–Ar age and IR emission spectrum of lunar granulite Northwest Africa 4881. *Lunar Planet. Sci. XL*, number 2009. Lunar Planet. Inst., Houston (abstr.).

Fernandes V. A., Fritz J., Wuenemann K. and Hornemann U. (2010) K-Ar ages and shock effects in lunar meteorites. *EPSC Abstracts* **5**, EPSC2010-237, European Planetary Science Congress.

Fernandes V. A., Fritz J., Weiss B., Garrick-Bethel and Shuster D. (2013) The bombardment history of the Moon as recorded by $^{40}Ar$-$^{39}Ar$ chronology. *Meteorit. Planet. Sci.* **48**, 241–269.

Floss C., James O. B., McGee J. J. and Crozaz G. (1998) Lunar ferroan anorthosite petrogenesis: clues from trace element distributions in FAN subgroups. *Geochim. Cosmochim. Acta* **62**, 1255–1283.

Fritz J., Greshake A. and Stöffler D. (2005a) Micro-Raman spectroscopy of plagioclase and maskelynite in Martian meteorites: Evidence of progressive shock metamorphism. *Antarct. Meteor. Res.* **18**, 96–116.

Fritz J., Greshake A. and Artemieva N. (2005b) Ejection of Martian meteorites. *Meteorit. Planet. Sci.* **40**, 1393–1411.

Fritz J., Wünnemann K., Greshake A., Fernandes V. A. S. M., Boettger U. and Hornemann U. (2011) Shock pressure calibration for lunar plagioclase, 42nd Lunar and Planetary Science Conference, #1196.

Gaffney A. M. and Borg, L. E. (2013) A young age for KREEP formation determined from Lu–Hf isotope systematics of KREEP basalts and Mg-suite samples. In: *44th Lunar Planetary Science Conference #1714*.

Gaffney A. M. and Borg L. E. (2014) A young solidification age for the lunar magma ocean. *Geochim. Cosmochim. Acta* **140**, 227–240.

Garrick-Bethell I., Nimmo F. and Wieczorek M. A. (2010) Structure and formation of the lunar farside highlands. *Science* **330**, 949–951.

Ghods A. and Arkani-Hamed J. (2007) Impact induced convection as the main mechanism for formation of lunar mare basalts. *J. Geophys. Res.-Plane.* **112**, E03005.

Gomes R., Levison H. F., Tsiganis K. and Morbidelli A. (2005) Origin of the cataclysmic Late Heavy Bombardment period of the terrestrial planets. *Nature* **435**, 466–469.

Grange M. L., Nemchin A. A., Pidgeon R. T., Timms N., Muhling J. R. and Kennedy A. K. (2009) Thermal history recorded by the Apollo 17 impact melt breccia 73217. *Geochim. Cosmochim. Acta* **73**, 3093–3107.

Gross J., Treiman A. H. and Mercer C. (2012) Lunar feldspathic meteorites: constraints on the geology of the lunar farside highlands and the origin of the lunar crust, Second Conference on the Lunar Highlands Crust, #9021.

Gross J., Treiman A. H. and Mercer C. N. (2014) Lunar feldspathic meteorites: constraints on the geology of the lunar highlands, and the origin of the lunar crust. *Earth Planet. Sc. Lett.* **388**, 318–328.

Halliday A. N. (2008) A young Moon-forming giant 70–110 million years accompanied by late-stage mixing, core formation and degassing of the Earth. *Philos. Trans. R. Soc.* **366**, 4163–4181.

Halliday A. N. and Porcelli D. (2001) In search of lost planets – the paleocosmochemistry of the inner solar system. *Earth Planet. Sci. Lett.* **192**, 545–559.

Harrison T. M., Schmitt A. K., McCulloch M. T. and Lovera O. M. (2008) Early ($\geqslant$ 4.5 Ga) formation of the terrestrial crust: Lu-Hf, $\delta^{18}O$, and Ti thermometry results for Hadean zircons. *Earth Planet. Sci. Lett.* **268**, 476–486.

Hawke B. R., Peterson C. A., Blewett D. T., Bussey D. B. J., Lucey P. G., Taylor G. J. and Spudis P. D. (2003) Distribution and modes of occurrence of lunar anorthosite. *J. Geophys. Res.* **108** (E6), 5050. http://dx.doi.org/10.1029/ 2002JE001890.

Hiesinger H. and Head J. (2006) New views in lunar geoscience: an introduction and overview, v. 60 of Reviews in Mineralogy &Geochemistry. *Mineral. Soc. Am.*

Hudgins J. and Spray J. (2009) Lunar Granulitic Breccias: Differences Between Apollo and Meteorite Samples, In 72nd Annual Meteoritical Society Meeting, #5157.

Hudgins J. A., Spray J. G., Kelley S. P., Korotev R. L. and Sherlock S. C. (2008) A laser probe $^{40}Ar/^{39}Ar$ and INAA investigation of four Apollo granulitic breccias. *Geochim. Cosmochim. Acta* **72**, 5781–5798.

Hudgins J., Kelley S. P., Korotev R. L. and Spray J. G. (2011a) Mineralogy, geochemistry, and $^{40}Ar$-$^{39}Ar$ geochronology of lunar granulitic breccia Northwest Africa 3163 and paired stones: Comparisons with Apollo samples. *Geochim. Cosmochim. Acta* **75**, 2865–2881.

Hudgins J. A., Spray J. G. and Hawkes C. D. (2011b) Element diffusion rates in lunar granulitic breccias: Evidence for contact metamorphism on the Moon. *Am. Mineral.* **96**, 1673–1685.

Hui H., Peslier A. H., Zhang Y. and Neal C. R. (2013) Water in lunar anorthosites and evidence for a wet early Moon. *Nat. Geosci.* **6**, 177–180.

Irving A. J., Kuehner S. M., Korotev R. L., Rumble, III, D. and Hupé G. (2006) Mafic Granulitic Impactite Northwest Africa 3163: A unique meteorite from the deep lunar crust, Lunar and Planetary Science Conference XXXVII. Abstract #1365.

Ishii T. (1975) The relations between temperature and composition of pigeonite in some lavas and their application to geothermometry. *Mineral. J.* **8**(1), 48–57.

Jacobson S. A., Morbidelli A., Rayond S. N., O'Brien D. P., Walsh K. J. and Rubie D. C. (2014) Highly siderophile elements in Earth's mantle as a clock for the Moon-forming impact. *Nature* **508**, 84–87.

James O. B. (1980) Rocks of the early lunar crust. In *Proceedings of the 11th Lunar and Planetary Science Conference*, pp. 365–393.

James O. B., Lindstrom M. M. and Flohr M. K. (1989) Ferroan anorthosite from lunar breccia 64435: Implications for the origin and history of lunar ferroan anorthosites, Proceedings of the 19th Lunar Planetary Science Conference, pp. 219–243.

James O. B., McGee J. J. and Lindstrom M. M. (1991) Lunar ferroan anorthosite 60025: Petrology and chemistry of mafic lithologies. *Proceedings of the Lunar and Planetary Science Conference* **21**, 63–87.

James O. , Cohen B. A. and Taylor L. A. (2003) Lunar Meteorite Dhofar 026: A shocked granulitic breccia, not an impact melt, 34th Lunar and Planetary Science Conference, #1149.

Jolliff B. L., Rockow K. M., Korotev R. L. and Haskin L. A. (1996) Lithologic distribution and geologic history of the Apollo 17 site: The record in soils and small rock particles from the highland massifs. *Meteorit. Planet. Sci.* **31**, 116–145.

Jolliff B .L., Wieczorek M. A., Shearer C. A. and Neal C. R., (eds.) (2006) New views of the moon. In: *Reviews in mineralogy and geochemistry*, vol. 60. Mineralogical Society of America, Washington, DC.

Joy K. H. and Arai T. (2013) Lunar meteorites: new insights into the geological history of the Moon. *Astron. Geophys.* **54**, 4.28–4.32.

Kent J. J., Brandon A. D., Lapen T. J., Peslier A. h., Irving A. J. and Coleff D. M. (2012) In-situ characterization of mineral phases in lunar granulite meteorite Northwest Africa 5744, 43rd Lunar and Planetary Science Conference, #2559.

Kleine T., Touboul M., Bourdon B., Nimmo F., Mezger K., Palme H., Jacobsen S. B., Yin Q.-Z. and Halliday A. N. (2009) Hf-W chronology of the accretion and early evolution of asteroids and terrestrial planets. *Geochim. Cosmochim. Acta* **73**, 5150–5188.

Koeberl C., Kurat G. and Brandstätter F. (1996) Mineralogy and geochemistry of lunar meteorite Queen Alexandra Range 93069. *Meteorit. Planet. Sci.* **31**, 897–908.

Korotev R. and Jolliff B. (2001) The curious case of the lunar magnesian granulitic breccias. *Lunar Planet. Sci. XXXII*, #1455. Lunar Planet. Inst., Houston (abstr.).

Korotev R., Jolliff B., Zeigler R., Gillis J. and Haskin L. (2003) Feldspathic lunar meteorites and their implications for compositional remote sensing of the lunar surface and the composition of the lunar crust. *Geochim. Cosmochim. Acta* **67**(24), 4895–4923.

Korotev R., Zeigler R. and Jolliff B. (2006) Feldspathic lunar meteorites Pescora Escarpment 02007 and Dhofar 489: Contamination of the surface of the lunar highlands by post-basin impacts. *Geochim. Cosmochim. Acta* **70**, 5935–5956.

Laneuville M., Wieczorek M. A., Breur D. and Tosi N. (2013) Asymmetric thermal evolution of the Moon. *J. Geophys. Res. Planets* **118**, 1435–1452.

Laul J. C., Smith M. R. and Schmitt R. A. (1983) Allan hills 81005: Petrology of a new lunar highland sample. *Geophys Res. Lett* **10**, 795–798.

Lindsley D. (1983) Pyroxene thermometry. *Am. Mineral.* **68**, 477–493.

Lindstrom M. and Lindstrom D. (1986) Lunar Granulites and Their Precursor Anorthositic Norites of the Early Lunar Crust. *J. Geophys. Res.* **91**(B4), D263–D276.

Lindstrom M. M. and Salpas P. A. (1983) Geochemical studies of feldspathic fragmental breccias and the nature of North Ray Crater Ejecta. *J. Geophys. Res.* **88**, A671–A683.

Lindstrom M. M., Schwarz C., Score R. and Mason B. (1991) MacAlpine Hills 88104 and 88105 lunar highland: General description and consortium overview. *Geochim. Cosmochim. Acta* **55**, 2999–3007.

Liu D., Jolliff B. L., Zeigler R. A., Korotev R. L., Wan Y., Xie H., Zhang Y., Dong C. and Wang W. (2012) Comparative zircon U-Pb geochronology of impact melt breccias from Apollo 12 and lunar meteorite SaU 169, and implications for the age of the Imbrium impact. *Earth Planet. Sci. Lett.* **319–320**, 277–286.

Ma M.-S. and Schmitt R. A. (1982) Chemistry of the matrix, the glass coating and an olivine clast from polymict ANT breccia 60035. In *Proceedings, 13th Lunar and Planetary Science Conference*, pp. 453–454.

Maloy A. K., Treiman A. H. and Shearer, Jr., C. K. (2005) A magnesian granulite clast in lunar meteorite ALHA81005 (abstract). In *Proceedings, 68th Annual Meeting of the Meteoritical Society*, #5278.

Marks N., Borg L., Gaffney A., Shearer C. and Burger P. (2014) Additional evidence for young ferroan anorthositic magmatism on the Moon from Sm–Nd isotopic measurements of 60016 Clast 3C. In *44th Lunar and Planetary Science Conference*, #1129.

Marvin U. B., Lindstrom M. M., Bernatowicz T. J., Podosek F. A. and Sugiura N. (1987) The composition and history of breccia 67015 from North Ray Crater. In *Proceedings of the 17th. Lunar and Planetary Science Conference, Journal of Geophysical Research*, 92, supplement: E471-E490.

Meyer C. (2009) Lunar sample compendium. http://curator.jsc.nasa.gov/lunar/ compendium.cfm.

Meyer C., Williams I. S. and Compston W. (1996) Uranium-lead ages for lunar zircons: evidence for a prolonged period of granophyre formation from 4.32 to 3.88 Ga. *Meteorit. Planet. Sci.* **31**, 370–387.

McGee J. J., Bence A. E. and Schaeffer O. A. (1978) Feldspathic granulite 79215: conditions of metamorphism and age. *Proceedings of Lunar Science Conference* **9**, 720–722.

McLeod C. L., Brandon A. D. and Armytage R. M. G. (2014) Constraints on the formation age and evolution of the Moon from $^{142}$Nd-$^{143}$Nd systematics of Apollo 12 basalts. *Earth Planet. Sci. Lett.* **396**, 179–189.

Meyer J., Elkins-Tanton L. T. and Wisdom J. (2010) Coupled thermal-orbital evolution of the early Moon. *Icarus* **208**, 1–10.

Minster J.-F., Birck J.-L. and Allegre C. J. (1982) Absolute age of formation of chondrites studied by the $^{87}$Rb-$^{87}$Sr method. *Nature* **300**, 414–419.

Nagaoka H., Karouji Y., Arai T., Ebihara M. and Hasebe N. (2013) Geochemistry and mineralogy of a feldspathic lunar meteorite (regolith breccia), Northwest Africa 2200. *Polar Sci.* **7**, 241–259.

Nemchin A., Timms N., Pidgeon R., Geisler, Reddy S. and Meyer C. (2009) Timing of crystallization of the lunar magma ocean constrained by the oldest zircon. *Nat. Geosci.* **2**, 133–136.

Norman M. D. and Ryder G. (1980) Geochemical evidence for the role of ilmenite and clinopyroxene in the early lunar differentiation. In *11th Lunar and Planetary Science Conference*, pp. 821–823.

Norman M. D., Keil K., Griffin W. L. and Ryan C. G. (1995) Fragments of ancient lunar crust: Petrology and geochemistry of ferroan noritic anorthosites from the Descartes region of the Moon. *Geochim. Cosmochim. Acta* **59**, 831–847.

Norman M. D., Borg L. E., Nyquist L. E. and Bogard D. D. (2003) Chronology, geochemistry, and petrology of a ferroan noritic anorthosite clast from Descartes breccia 67215: Clues to the age, origin, structure, and impact history of the lunar crust. *Meteorit. Planet. Sci.* **38**, 645–661.

Norman M. D., Duncan R. A. and Huard J. J. (2010) Imbrium provenance for the Apollo 16 Descartes terrain: Argon ages and geochemistry of lunar breccias 67016 and 67455. *Geochimica. Cosmochim. Acta* **74**, 763–783.

Norman M., Taylor L. A., Shih C.-Y. and Nyquist L. E. (2016) Crystal accumulation in a 4.2 Ga lunar impact melt. *Geochim. Cosmochim. Acta* **172**, 410–429.

Nunes P. D., Tatsumoto M. and Unruh D. M. (1975) U-Th–Pb systematics of anorthositic gabbros 78155 and 77017—impli-

cations for early lunar evolution. *Proceedings of Lunar Science Conference* **6**, 1445–1465.
Nyquist L. E. (1977a) Sr-isotopic constraints on the petrogenesis of Apollo 12 mare basalts. In *Proceedings of the 8th Lunar Science Conference*, pp. 1383–1415.
Nyquist L. E. (1977b) Lunar Rb-Sr chronology. *Phys. Chem. Earth* **10**, 103–142.
Nyquist L. E., Wiesmann H., Bansai B., Shih C.-Y., Keith J. E. and Harper C. L. (1995) $^{146}$Sm-$^{142}$Nd formation interval for the lunar mantle. *Geochim. Cosmochim. Acta* **59**, 2817–2837.
Nyquist L., Bogard D., Yamaguchi A., Shih C.-Y., Karouji Y., Ebihara M., Reese Y., Garrison D., McKay G. and Takeda H. (2006) Feldspathic clasts in Yamato-86032: Remnants of the lunar crust with implications for its formation and impact history. *Geochim. Cosmochim. Acta* **70**, 5990–6015.
Nyquist L. E., Shih C.-Y., Reese Y. D., Park J., Bogard D. D., Garrison D. H. and Yamaguchi A. (2010) Lunar crustal history recorded in lunar anorthosites. In *41st Lunar and Planetary Science Conference*, #1383.
Oberli F., Huneke J. C., McCulloch M. T., Papanastassiou D. A. and Wasserburg G. J. (1979) Isotopic constraints for the early evolution of the Moon. *Meteoritics* **14**, 502–503.
Ozima M. and Podosek F. A. (1999) Formation age of Earth from $^{129}$I/$^{127}$I and $^{244}$Pu/$^{238}$U systematics and the missing Xe. *J. Geophys. Res.* **104**, 25493–25499.
Palme H., Spettel B., Jochum K. P., Dreibus G., Weber H., Weckwerth G., Wänke, Bischoff A. and Stöffler D. (1991) Lunar highland meteorites and the composition of the lunar crust. *Geochim. Cosmochim. Acta* **55**, 3105–3122.
Papanastassiou D. A. and Wasserburg G. J. (1978) Strontium isotopic anomalies in the Allende Meteorite. *Geophys. Res. Lett.* **5**, 595–598.
Papike J., Karner J. and Shearer C. (2003) Determination of planetary basalt parentage: A simple technique using the electron microprobe. *Am. Mineral.* **88**, 469–472.
Pernet-Fischer J. and Joy K. H. (2016) The lunar highlands: old crust, new ideas. *Astron. Geophys.* **57**, 1.26–1.30.
Phinney D., Kahl S. B. and Reynolds J. H. (1975) $^{40}$Ar–$^{39}$Ar dating of Apollo 16 and 17 rocks. *Proceedings of Lunar Science Conference* **6**, 1593–1608.
Pidgeon R. T., Nemchin A. A., van Bronswijk W., Geisler T., Meyer C., Compston W. and Williams I. S. (2007) Complex history of a zircon aggregate from lunar breccia 73235. *Geochim. Cosmochim. Acta* **71**, 1370–1381.
Podosek F. A., Zinner E. K., MacPherson G. J., Lundberg L. L., Brannon J. C. and Fahey A. J. (1991) Correlated study of initial $^{87}$Sr/$^{86}$Sr and Al-Mg isotopic systematics and petrologic properties in a suite of refractory inclusions from the Allende meteorite. *Geochim. Cosmochim. Acta* **55**, 1083–1110.
Rankenburg K., Brandon A. D. and Neal C. R. (2006) Neodymium Isotope Evidence for a Chrondritic Composition of the Moon. *Science* **312**, 1369–1372.
Renne, Swisher P. R. C. C., Deino A. L., Karner D. B., Owens T. L. and DePaolo D. L. (1998) "Intercalibration of Standards, Absolute Ages and Uncertainties in $^{40}$Ar/$^{39}$Ar Dating. *Chem. Geol.* **145**, 117–152.
Renne P. R., Balco G., Ludwig K. R., Mundil R. and Min K., et al. (2011) Response to the comment by W.H. Schwarz, on "Joint determination of 40K decay constants and 40Ar$^*$/40K for the Fish Canyon sanidine standard, and improved accuracy for 40Ar/39Ar geochronology" by P.R. Renne et al. (2010). *Geochim. Cosmochim. Acta* **75**, 5097–5100.
Rubin A. E. (2015) Maskelynite in asteroidal, lunar and planetary basaltic meteorites: An indicator of shock pressure during impact ejection from their parent bodies. *Icarus* **257**, 221–229.
Ryder G. (1982) Lunar anorthosite 60025, the petrogenesis of lunar anorthosites, and the composition of the moon. *Geochim. Cosmochim. Acta* **46**, 1591–1601.
Ryder G., Norman M. D. and Taylor G. J. (1997) The complex stratigraphy of the highland crust in the Serenitatis region of the Moon inferred from mineral fragment chemistry. *Geochim. Cosmochim. Acta* **61**, 1083–1105.
Salpas P. A., Lindstrom M. M. and Taylor L. A. (1988) Highland materials at Apollo 17: contributions from 72275. In *Proceedings, 18th Lunar and Planetary Science Conference*, pp. 11–19.
Schaeffer O. A. and Schaeffer G. A. (1977) $^{39}$Ar–$^{40}$Ar ages of lunar rocks. In *Proceedings of the 4th Lunar Science Conference*, 8, pp. 840–842. Proceedings of the 4th Lunar Science Conference. Lunar Planetary Institute, Houston.
Schwarz W. H. and Trieloff M. (2007) Intercalibration of $^{40}$Ar–$^{39}$Ar age standards NL-25, HB3gr hornblende, GA1550, SB-3, HD-B1 biotite and BMus/2 muscovite. *Chem. Geol.* **242**, 218–231.
Schwarz W. H., Kossert K., Trieloff M. and Hopp J. (2011) Comment on the "Joint determination of $^{40}$K decay constants and $^{40}$Ar$^*$/$^{40}$K for the Fish Canyon sanidine standard, and improved accuracy for $^{40}$Ar/$^{39}$Ar geochronology" by Paul R. Renne et al. (2010). *Geochim. Cosmochim. Acta* **75**, 5094–5096.
Shearer C. K., Elardo S. M., Petro N. E., Borg L. E. and McCubbin F. (2015) Origin of the lunar highlands Mg-suite: an integrated petrology, geochemistry, chronology, and remote sensing perspective. *Am. Mineral.* **100**, 294–325.
Shuster D. L., Balco G., Cassata W. S., Fernandes V. A., Garrick-Bethell I. and Weiss B. P. (2010) A record of lunar impacts preserved in the lunar regolith. *Earth Planet. Sci. Lett.* **290**, 155–165.
Smith J. V., Andersen A. T., Newton R. C., Olsen E. J., Crewe A. V., Isaacson M. S., Johnson D. and Wyllie P. J. (1970) Petrologic history of the Moon inferred from petrography, mineralogy and petrogenesis of the Apollo 11 rocks. In *Proceedings of the Apollo 11 Lunar Science Conference*. Pergamon, New York, pp. 897–926.
Snyder G. A., Borg L. E., Nyquist L. E. and Taylor L. A. (2000) Chronology and isotopic constraints on lunar evolution. In *On Origin of the Earth and Moon* (eds. R. A. Canup and K. Righter), pp. 361–395.
Solomon S. (1975) Mare volcanism and lunar crustal structure. *Lunar Planet. Sci. VI*, 762–764.
Stettler A., Eberhardt P., Geiss J., Grögler N. and Maurer P. (1973) 40Ar–39Ar ages and 37Ar–38Ar exposure ages of lunar rocks. In *Proceedings of the 4th Lunar Science Conference*, 4, pp. 1865–1888. Proceedings of the 4th Lunar Science Conference. Lunar Planetary Institute, Houston.
Stöffler D., Ostertag R., Jammes C., Pfannschmidt G., Sen Gupta P., Simon S., Papike J. and Beauchamp R. (1986) Shock metamorphism and petrography of the Shergotty achondrite. *Geochim. Cosmochim. Acta* **50**, 889–903.
Taylor S. R. (1982) *Planetary Science: A Lunar Perspective*. Lunar Planetary Institutes, Houston, TX.
Taylor G. J. (2009) Ancient Lunar Crust: Origin, Composition, and Implications. *Elements* **5**, 17–22.
Taylor S. R. and McClennan S. M. (1985) *The Continental Crust: Its Composition and Evolution*. Blackwell, Oxford, p. 312.
Thirlwall M. F. (1991) Long-term reproducibility of multicollector Sr and Nd isotope ratio analysis. *Chem. Geol.* **94**, 85–104.
Touboul M., Kleine T., Bourdon B., Palme H. and Wieler R. (2007) Late formation and prolonged differentiation of the Moon inferred from W isotopes in lunar metals. *Nature* **450**, 1206–1209.
Turner G. and Cadogan P. H. (1975) The history of lunar bombardment inferred from $^{40}$Ar-$^{39}$Ar dating of highland rocks. In: *Proceedings, 5th Lunar Science Conference*. pp. 1509–1538.

Valley J. W., Cavosie A. J., Ushikubo T., Reinhard D. A., Lawrence D. F., Larson D. J., Clifton P. H., Kelly T. F., Wilde S. A., Moser D. E. and Spicuzza M. J. (2014) Hadean age for a post-magma-ocean zircon confirmed by atom-probe tomography. *Nat. Geosci.* **7**, 219–223.

Warner J., Phinney W., Bickel C. and Simonds C. (1977) Feldspathic granulitic impactites and pre-final bombardment lunar evolution. *Proceedings of the Lunar and Planetary Science Conference* **8**, 2051–2066.

Warren P. H. (1990) Lunar Anorthosites and the magma-ocean plagioclase-flotation hypothesis: Importance of FeO enrichment in the parent magma. *Am. Mineral.* **75**, 46–58.

Warren P. H. (2005) "New" lunar meteorites: Implications for composition of the global lunar surface, lunar crust, and the bulk Moon. *Meteorit. Planet. Sci.* **40**(3), 477–506.

Warren P. H. and Kallemeyn G. W. (1993) The Ferroan-Anorthositic Suite, the Extent of Primordial Lunar Melting and the Bulk Composition of the Moon. *J. Geophys. Res.* **98**, 5445–5455.

Warren P. H. and Taylor G. R. (2013) The moon. In *Treatise on Geochemistry* (eds. H. Holland and Turekian), p. 9144, second ed.

Warren P. H. and Wasson J. T. (1977) Pristine nonmare rocks and the nature of the lunar crust. In *Proceedings of the 8th Lunar Science Conference*, pp. 2215–2235.

Werner S. C. (2014) Moon, Mars, Mercury: Basin formation ages and implications for the maximum surface age and the migration of gaseous planets. *Earth Planet. Sci. Lett.* **400**, 54–65.

Wilcox B., Robinson M., Thomas P. and Hawke B. (2005) Constraints on the depth and variability of the lunar regolith. *Meteorit. Planet. Sci.* **40**(5), 695–710.

Wood J. A., Dickey J. S., Marvin U. B. and Powell B. N. (1970) Lunar anorthosites and a geophysical model of the Moon. In *Proceedings of the Apollo 11 Lunar Science Conference*. Pergamon, New York, pp. 965–988.

Zhang N., Parmentier E. M. and Liang Y. (2013) A 3-D numerical study of the thermal evolution of the Moon after cumulate mantle overturn: The importance of rheology and core solidification. *J. Geophys. Res. Planets* **118**, 1789–1804.

*Associate editor:* Marc Norman